Progress in Solid State Chemistry 37 (2009) 132–152

Contents lists available at ScienceDirect

Progress in Solid State Chemistry

journal homepage: www.elsevier.com/locate/pssc

Thermodynamics, structure and kinetics in the system Ga–O–N

Manfred Martin [a,*], Richard Dronskowski [b], Jürgen Janek [c], Klaus-Dieter Becker [d], Daniel Roehrens [a], Jochen Brendt [a], Marck W. Lumey [b], Lakshmi Nagarajan [a], Ilia Valov [c], Alexander Börger [d]

[a] Institut für Physikalische Chemie, RWTH Aachen University, Landoltweg 2, D-52056 Aachen, Germany
[b] Institut für Anorganische Chemie, RWTH Aachen University, Landoltweg 1, D-52056 Aachen, Germany
[c] Physikalisch-Chemisches Institut, Justus-Liebig-Universität Gießen, Heinrich-Buff-Ring 58, D-35392 Gießen, Germany
[d] Institut für Physikalische und Theoretische Chemie, TU Braunschweig, Hans-Sommer-Str. 10, D-38106 Braunschweig, Germany

Keywords:
β-Ga_2O_3
GaN
Ga–O–N
GaO_x
GaO_xN_y
Ammonolysis
Oxynitrides
Nitrogen solubility
γ-Galon
In situ XAS
Nucleation
Non-stoichiometry
Amorphous oxide
Insulator–metal transition

A B S T R A C T

Within the ternary system Ga–O–N we performed experimental and theoretical investigations on the thermodynamics, structure and kinetics of new stable and metastable compounds.

We studied the ammonolysis of β-Ga_2O_3 at elevated temperatures by means of *ex situ* X-ray diffraction, *ex situ* neutron diffraction, and *in situ* X-ray absorption spectroscopy (XAS). From total diffraction pattern refinement with the Rietveld method we analyzed the anionic occupancy factors and the lattice parameters of β-Ga_2O_3 during the reaction. Within the detection limits of these methods, we can rule out the existence of a crystalline oxynitride phase that is not derived from wurtzite-type GaN. The nitrogen solubility in β-Ga_2O_3 was found to be below the detection limit of about 2–3 at.% in the anionic sublattice. The kinetics of the ammonolysis of β-Ga_2O_3 to α-GaN and of the oxidation of α-GaN to β-Ga_2O_3 was studied by means of *in situ* X-ray absorption spectroscopy. In both cases the reaction kinetics could be described well by fitting linear combinations of β-Ga_2O_3 and α-GaN spectra only, excluding that other crystalline or amorphous phases appear during these reactions. The kinetics of the ammonolysis can be described well by an extended Johnson–Mehl–Avrami–Kolmogorow model with nucleation and growth of GaN nuclei, while the oxidation kinetics can be modeled by a shrinking core model where Ga_2O_3 grows as a layer. Investigations by means of TEM and SEM support the assumptions in both models.

To investigate the structure and energetics of spinel-type gallium oxynitrides (γ-galons) we performed first-principles calculations using density-functional theory. In addition to the ideal cubic γ-Ga_3O_3N we studied gallium deficient γ-galons within the Constant-Anion-Model.

In highly non-stoichiometric, amorphous gallium oxide of approximate composition $GaO_{1.2}$ we found at a temperature around 670 K an insulator–metal transition, with a conductivity jump of seven orders of magnitude. We demonstrate through experimental studies and density-functional theory calculations that the conductivity jump takes place at a critical gallium concentration and is induced by crystallization of stoichiometric β-Ga_2O_3 within the metastable oxide matrix. By doping with nitrogen the critical temperature and the conductivity in the highly conducting state can be tuned.

Contents

* Corresponding author. Tel.: +49 241 8094712; fax: +49 241 8092128.
E-mail address: martin@rwth-aachen.de (M. Martin).

0079-6786/$ – see front matter © 2009 Elsevier Ltd. All rights reserved.
doi:10.1016/j.progsolidstchem.2009.11.005

1. Introduction

Recent developments have shown increased interest in gallium oxide and gallium nitride compounds as base materials for (opto-) electronic components such as light emitting diodes or sensors [1–5]. Both compounds belong to the system Ga–O–N the phase diagram of which is shown schematically as a Gibbs triangle in Fig. 1. In the third dimension, either the temperature or the pressure could be plotted. At ambient pressure of 1 bar, only two thermodynamically stable phases are known, β-Ga_2O_3 and α-GaN.

While there have been extensive efforts in researching the binary compounds β-Ga_2O_3 and α-GaN, there is only a small number of reports on potential gallium oxynitrides that are either intermediate compounds in the quasi-binary system Ga_2O_3–GaN (located on the dashed line in Fig. 1) or real ternary compounds GaO_xN_y (located offside the dashed line). Most of these studies focus on compounds to be found at the nitrogen-rich side of the quasi-binary system. These N-rich oxynitrides are characterized as being derived from wurtzite-type GaN, with dissolved oxygen in the anionic sublattice [6–13].

In this paper we summarize our recent experimental and theoretical investigations within the ternary system Ga–O–N. After reviewing in Section 2 the main crystallographic, physical, and chemical properties of the stable compounds β-Ga_2O_3 and α-GaN, we discus in Section 3 the ammonolysis of β-Ga_2O_3 in detail, concerning its thermodynamics and kinetics as well. In Section 4 we report our theoretical results on spinel-type gallium oxynitrides (γ-galons) and wurtzite-type, doped, nitrogen-rich oxynitrides. Finally, in Section 5, we leave the field of stoichiometric compounds within the ternary system Ga–O–N and investigate amorphous gallium excess compounds GaO_xN_y which show an unprecedented insulator–metal transition upon heating.

2. The stable compounds β-Ga_2O_3 and α-GaN

2.1. β-Ga_2O_3

Under standard conditions β-Ga_2O_3 is the thermodynamically stable phase in the Ga–O system [14,15]. It crystallizes in the monoclinic crystal system (C2/m). There are two cation positions, one is octahedrally the other is tetrahedrally coordinated. For the anion sites there are three crystallographically different positions, whereupon two are coordinated trigonally and one is coordinated tetrahedrally. The structure according to Åhman et al. [16] is shown in Fig. 2 and crystallographic data is summarized in Table 1.

β-Ga_2O_3 is a very stable compound with a large Gibbs energy of formation, $\Delta_f G^0(T = 1000\ \mathrm{K}) = -760\ \mathrm{kJ\ mol^{-1}}$ [17]. It is a wide-gap, n-type semiconductor with an optical band gap of 4.9 eV [18]. β-Ga_2O_3 has applications as a luminescent phosphor [19], as an oxygen sensor [3,20], as a deep-ultraviolet transparent oxide [21], and in different high temperature electronic applications [22]. β-Ga_2O_3 exhibits a slight oxygen-deficiency that is generally interpreted in terms of oxygen vacancies [23,24].

2.2. α-GaN

Under standard conditions α-GaN is the thermodynamically stable phase in the Ga–N system [25]. It crystallizes in the hexagonal wurtzite structure in which both Ga and N atoms are coordinated tetrahedrally. The structure according to Juza and Hahn [26] is shown in Fig. 3 and crystallographic data is summarized in Table 2.

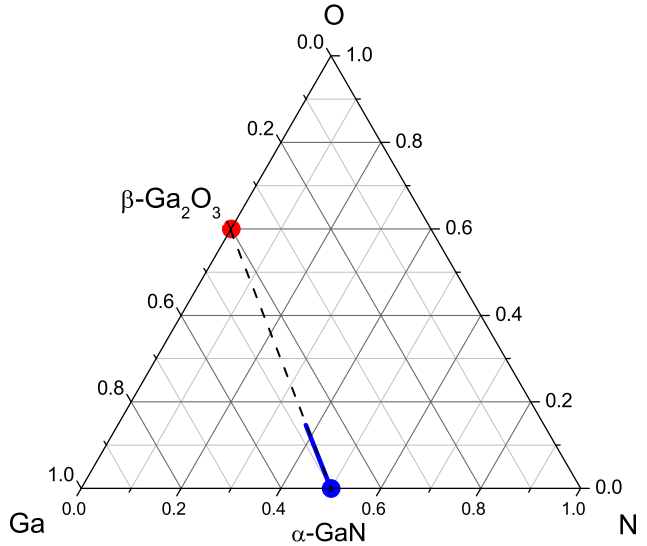

Fig. 1. The system Ga–O–N exhibits at ambient pressure only two thermodynamically stable compounds, β-Ga_2O_3 and α-GaN. The dashed line indicates the quasi-binary system formed by both compounds. The high solubility of Ga_2O_3 in GaN is indicated by the blue line. (For interpretation of the references to color in this figure legend, the reader is referred to the web version of this article.)

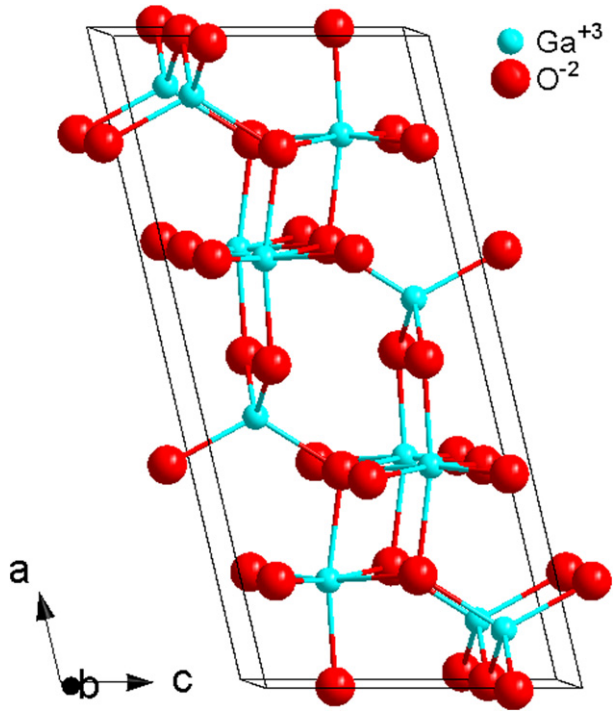

Fig. 2. Crystal structure of β-Ga_2O_3 from crystallographic data determined by Åhman et al. [16].

α-GaN is less stable than β-Ga_2O_3 with a Gibbs energy of formation, $\Delta_f G^0(T = 1000\ \mathrm{K}) = -20\ \mathrm{kJ\ mol^{-1}}$ [17]. It is an n-type semiconductor with an optical band gap of 3.5 eV [27]. α-GaN serves as basic material for different optoelectronic devices, especially for light emitting diodes (LEDs) with blue and ultraviolet light emission [2,28]. Other applications of α-GaN are heterostructure field effect transistors or Schottky rectifiers. It is well known, that the anion sublattice of GaN can accommodate up to 30 at.% of oxygen [6–13].

3. Ammonolysis of Ga_2O_3

A common way of synthesizing α-GaN is the ammonolysis of β-Ga_2O_3:

Table 1
Crystallographic data of β-Ga_2O_3 according to Åhman et al. [16].

Phase					β-Ga_2O_3
Crystal System					monoclinic
Space Group					C 1 2/m 1
a [Å]					12.214(3)
b [Å]					3.0371(9)
c [Å]					5.7981(9)
Beta [°]					103.83(2)
Cell Volume [Å^3]					208.8
Formula Units					4
General Multiplicity					8
Atom	Wyckoff position	*x*	*y*	*z*	Site occupancy factor
Ga1	4i	0.09050(2)	0.0	0.79460(5)	0.5
Ga2	4i	0.15866(2)	0.5	0.31402(5)	0.5
O1	4i	0.1645(2)	0.0	0.1098(3)	0.5
O2	4i	0.1733(2)	0.0	0.5632(4)	0.5
O3	4i	−0.0041(2)	0.5	0.2566(3)	0.5

Site occupancy factors are determined by dividing the Wyckoff number of an atom position by the general multiplicity. A site occupancy factor 0.5 corresponds to a fully occupied site.

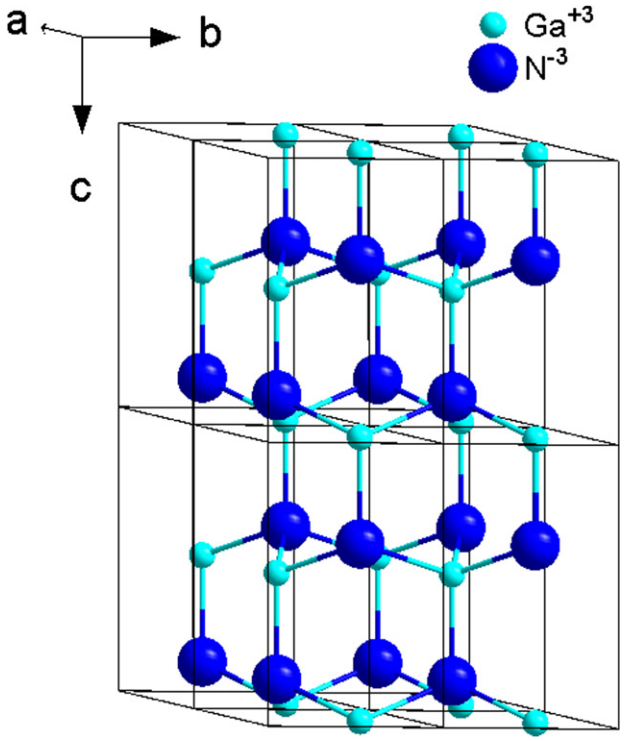

Fig. 3. Crystal structure of α-GaN from crystallographic data determined by Juza and Hahn [26].

$$Ga_2O_3 + 2NH_3 \rightarrow 2GaN + 3H_2O \quad \text{(I)}$$

The reaction is accomplished by flowing ammonia over β-Ga_2O_3 powder in a temperature range between 873 and 1373 K [29,30]. For this conversion from the oxide to the nitride, gallium oxynitrides were postulated as reaction intermediates [31]. Although the ammonolysis of β-Ga_2O_3 is of such enormous importance, systematic and quantitative studies of the reaction mechanism and the reaction kinetics are scarce. In the subsequent Sections 3.1 and 3.2 we will summarize our recent investigations of the ammonolysis reaction which were performed by *ex situ* X-ray and neutron diffraction [32] and *in situ* X-ray absorption spectroscopy [33] to confirm or disprove the existence of gallium oxynitrides.

3.1. Phase analysis by means of XRD and neutron diffraction

For the qualitative phase analysis and the monitoring of the lattice parameters during ammonolysis we conducted *ex situ* XRD

Table 2
Crystallographic data for α-GaN according to Juza and Hahn [26]. The site occupancy of 1/6 corresponds to full occupation (see caption of Table 1 for explanation).

Phase					GaN
Crystal System					hexagonal
Space Group					P 6_3 m c
a [Å]					3.180(4)
b [Å]					3.180(4)
c [Å]					5.166(5)
Cell Volume [Å^3]					45.2
Formula Units					2
General Multiplicity					12
Atom	Wyckoff position	*x*	*y*	*z*	Site occupancy factor
Ga	2b	1/3	2/3	0	1/6
N	2b	1/3	2/3	3/8	1/6

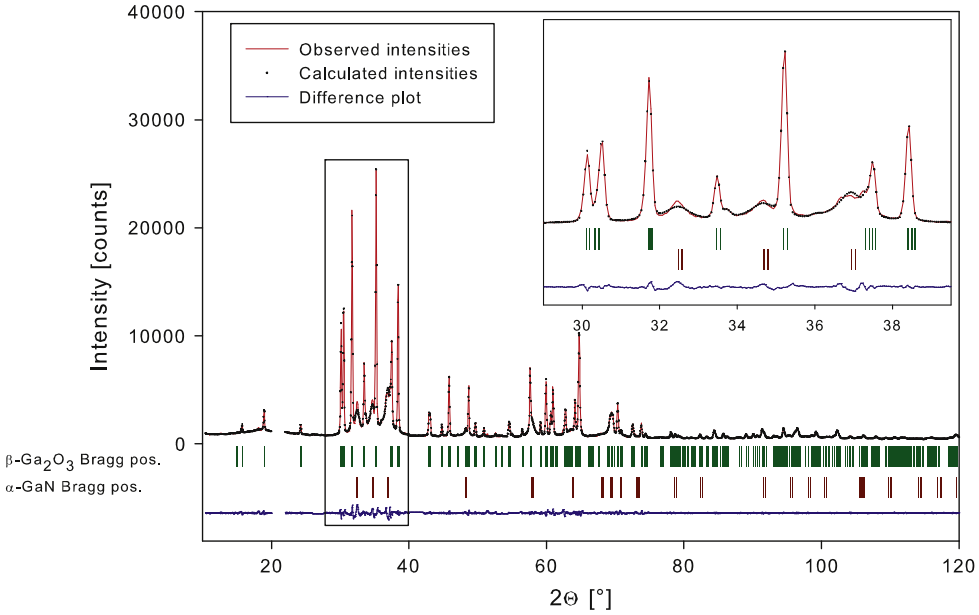

Fig. 4. Observed and refined XRD intensities of a β-Ga_2O_3 sample that was ammonolyzed for 24 h at 873 K (resulting in 59.5 mol% GaN, see Table 3). The inset shows a zoom into the 2θ region between 28° and 42°. The region between 20° and 22° is excluded due to a contribution from the glue used to prepare the sample for the measurement.

experiments on quenched powder samples. In order to detect any nitrogen within the ammonolyzed β-Ga_2O_3-phase, *ex situ* neutron diffraction experiments on quenched powder samples were carried out.

In our experiments, all powder samples were prepared from commercially available Ga_2O_3 powder (Alfa Aesar, Puratronic) by pre-sintering for 48 h at 1598 K in air to ensure phase purity of the β-phase and to increase the crystallite size to a level where diffraction line broadening is negligible. Subsequently, ammonolysis of the samples was carried out at different temperatures (803–923 K) and for reaction times up to 48 h, as described in detail in Ref. [32].

Conventional X-ray diffraction techniques were used to characterize the crystalline samples. Diffraction patterns were recorded on a transmission diffractometer (Stadi-P, STOE Darmstadt, Germany) that is equipped with a primary Ge (111) monochromator and a scintillation counter with graphite secondary monochromator. All measurements were performed with Cu $K\alpha_1$ radiation ($\lambda = 1.540598$ Å). The XRD patterns were collected in a 2θ-range from 10 to 120° in steps of 0.05° in order to ensure a sufficient quality of the refinement.

Constant wavelength neutron diffraction was carried out at the SPODI neutron powder diffractometer at the FRMII reactor in Garching, Germany. It is equipped with a vertically focusing monochromator that consists of 17 Ge (551) crystals and 80 ^{3}He detectors. A 2θ-range of 160° is covered, and the diffraction data were afterwards corrected for beam divergence.

Rietveld refinement of XRD and neutron data was carried out with the Fullprof software package using the Thompson-Cox-Hastings Pseudo-Voigt profile function [34]. For each experimental setup, a preceding profile matching routine was applied. The profile parameters thus acquired were used as starting values for each structural refinement. From the pattern matching calculations we extracted the refined lattice parameters, while the quantitative phase composition and atomic parameters where obtained from the structural refinements. The background was fitted as linear interpolation between a set of chosen background points with refineable heights. The neutron wavelength was refined with a standard sample to $\lambda = 1.547466(9)$ Å.

3.1.1. X-ray diffraction

Fig. 4 shows a typical XRD pattern together with the refined intensities for a β-Ga_2O_3 sample that was ammonolyzed for 24 h at 873 K. Apart from the monoclinic β-Ga_2O_3 and hexagonal α-GaN no other phases can be detected in the diffraction pattern. The refinement of the lattice parameters of β-Ga_2O_3 shows no appreciable change compared to the values before the ammonolysis, indicating a very small solubility of nitrogen in the oxygen sublattice of β-Ga_2O_3. These findings apply to all of our ammonolysis experiments (see as an example Table 3 and in more detail Ref. [32]) from which we conclude that the ammonolysis of β-Ga_2O_3 leading to GaN does not proceed via (meta-) stable crystalline intermediates as had been suggested earlier [31].

From the GaN peaks we could extract its volume weighted average particle size, which shows the nitride phase to be nanocrystalline, e.g. with an average diameter $<D>_V = (20 \pm 5)$ nm in sample 5, assuming spherical particles. This is confirmed by

Table 3
Ammonolysis of β-Ga_2O_3 at 873 K for different durations. Refined cell parameters of β-Ga_2O_3 and amount of GaN as obtained by Rietveld refinement of the XRD data; (n.d.: not detectable).

Sample	Ammonolysis [h]	Rwp	Chi^2	Cell volume [Å^3]	*a* [Å]	*b* [Å]	*c* [Å]	mol% GaN
1	0	7.27	3.08	215.23471(31)	12.21644(18)	3.0365(5)	5.80222(9)	n.d.
2	3	6.55	1.52	215.45453(24)	12.21740(14)	3.03820(3)	5.80446(7)	n.d.
3	6	6.85	2.24	215.46331(22)	12.21797(13)	3.03827(3)	5.80427(6)	n.d.
4	14.5	6.22	2.12	215.31308(20)	12.21427(11)	3.03778(3)	5.80291(5)	10.0(0.3)
5	24	9.50	3.54	215.45645(44)	12.21613(27)	3.03869(6)	5.80417(11)	59.5(0.8)
6	48	14.8	8.37	215.64534(54)	12.2153(28)	3.03840(10)	5.8101(15)	96.1(1.4)

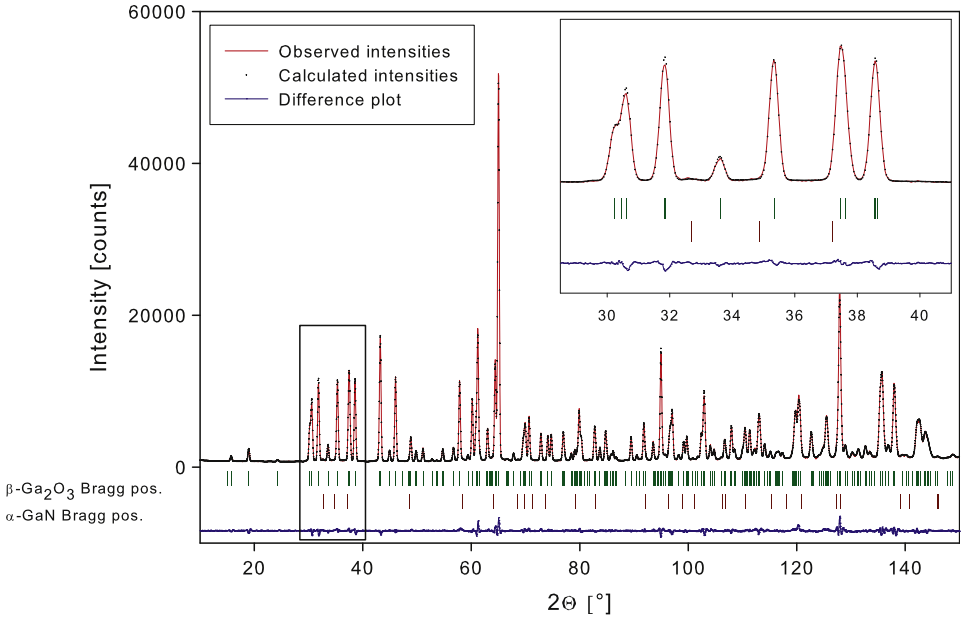

Fig. 5. Refinement of the neutron diffraction pattern of a β-Ga_2O_3 sample which has been ammonolyzed at 1053 K for 30 min (resulting in 8.6 mol% GaN, see Table 4). The inset shows a zoom into the 2θ region between 24° and 46°.

application of the same method to the neutron diffraction data (see 3.1.2) and is consistent with our findings from TEM investigations [33] (see also Section 3.3).

3.1.2. Neutron diffraction

In contrast to the X-Ray scattering factors of oxygen and nitrogen which are nearly identical, the coherent neutron scattering lengths of ^{14}N (9.370 fm) is much larger than that of ^{16}O (5.803 fm). Thus, any significant amount of nitrogen in the β-Ga_2O_3 lattice – on any oxygen site, either randomly distributed or preferentially located on a specific site – should show up in an effective occupancy factor that is larger than 0.5 (see Table 1). Considering for the noise in the diffraction patterns, a value of 3% nitrogen substituted for oxygen on any anion site seems to be a reasonable value for the detection limit above which any effect could be regarded as significant [32].

The refinements of the experimental diffraction patterns (see Fig. 5 as an example) show, however, no evidence of nitrogen on any site. If the nitrogen atoms were positioned on previously empty, interstitial sites, the powder pattern would show significant changes in the relative intensities even if symmetry is retained. This case can be ruled out by our data, which show the characteristic profile and intensity ratios of β-Ga_2O_3, with GaN being the only additional phase. In summary, the refined anionic occupancy factors of the oxide phase reveal no significant deviation from the theoretical value of 0.5 which represents a fully occupied position. Since this is the case for all our investigated samples (see Table 4) we can rule out that a significant amount of nitrogen (>3%) can be doped into β-Ga_2O_3 by means of ammonolysis. This conclusion is supported by the fact that the obtained lattice parameters of the oxide phase (see Fig. 6) do not show any significant trend towards lattice expansion or contraction in agreement with the XRD data.

Table 4
Ammonolysis of β-Ga_2O_3 at 1053 K for different durations. Effective occupancy factors of oxygen positions in β-Ga_2O_3 and amount of GaN as obtained from the refinement of the neutron diffraction data (n.d.: not detectable).

Ammonolysis [min]	Effective occupancy factors of O-positions in β-Ga_2O_3			mol% GaN
	O1	O2	O3	
0	0.504(4)	0.503(3)	0.507(5)	n.d.
5	0.505(4)	0.504(3)	0.507(4)	n.d.
15	0.506(4)	0.502(3)	0.507(4)	n.d.
30	0.506(4)	0.502(4)	0.507(4)	8.6(0.7)
120	0.505(5)	0.498(5)	0.504(5)	22.7(2.3)

3.2. Reaction kinetics by means of in situ X-ray absorption spectroscopy

To investigate the *kinetics* of the ammonolysis of Ga_2O_3 under *in situ* conditions, we used X-ray absorption spectroscopy (XAS) [33]. The XAS experiments were performed at beamlines C and X at HASYLAB (Hamburg, Germany) in transmission geometry. Measurements have been done on the Ga *K*-edge (10 367 eV), using Si (111) double crystal monochromators. As energy reference a pellet of the intermetallic compound CoGa diluted with BN was used [35]. For filtering higher harmonics, the monochromator was detuned to 60% of the maximum intensity.

The flow rates of the used gases (He, O_2, NH_3) were controlled by three mass flow controllers (MFC, each with 100 ml min^{-1}). The gas-tight furnace consists of a 250 mm long corundum tube with an inner diameter of 14 mm. Water cooled flanges with Kapton windows allow the X-rays to pass the furnace. Heating was done by a platinum wire around the corundum tube, which allows operating up to temperatures of 1473 K [36].

In each experiment, 5 mg of single-phase β-Ga_2O_3 (see 3.1) were mixed with 40 mg BN-powder and filled into the sample holder consisting of MACOR-ceramics. In front of and behind the sample, BN windows are used to hold the powder in position. Transport of the reactive gas to the powder particles is ensured by holes in the sample holder.

The ammonolysis of Ga_2O_3 according to reaction (I) was performed with pure ammonia gas at reaction temperatures of 933, 1053, and 1113 K. In all experiments the flow rates of ammonia respectively oxygen were set to 30 ml min^{-1}, and the sample

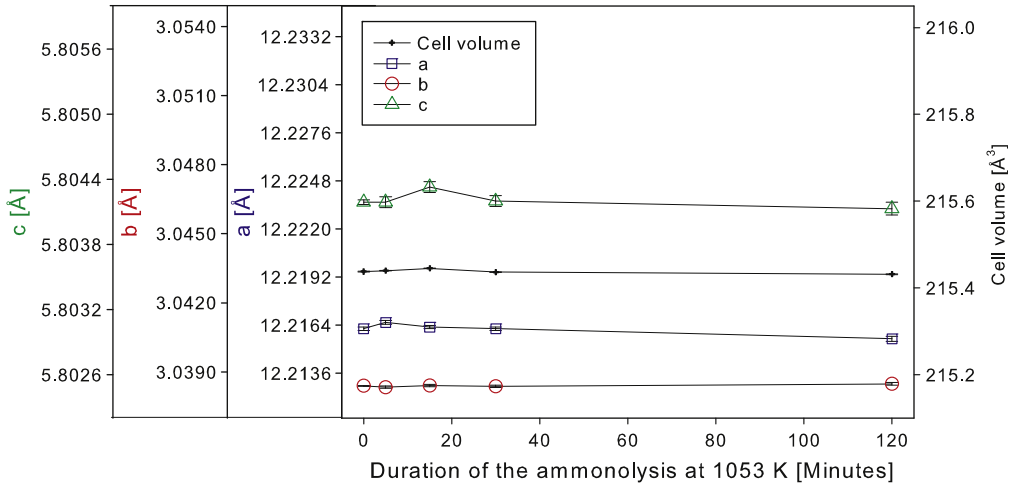

Fig. 6. Dependence of the refined cell parameters of β-Ga_2O_3 on the duration of the ammonolysis at 1053 K, obtained from neutron diffraction data refinement.

temperature was measured with a thermocouple in close vicinity of the sample.

The spectra on the Ga *K*-edge were measured over an energy range from 10 167 to 11 267 eV. Two different measurement modes were used. The Quick scanning EXAFS mode (QEXAFS) [37] was applied to analyze the reaction kinetics *in situ*. Conventional step-scanning EXAFS was used to record structural changes. Here, the reaction was quenched after 5 min by changing the gas atmosphere to Helium. After recording the spectrum (measuring time per data point = 1 s, energy step size = 5 eV in the prepeak region, 0.5 eV in the edge region, and 1 eV in the EXAFS region), another 5 min reaction/XAS spectrum cycle was done, until 5 or more consecutive spectra showed no further changes.

The analysis of the XAS raw data was done with the program Athena [38], according to the standard XAS procedures [39]. Data smoothing was performed with a 3-point adjacent averaging cycle with three iterations. The energy scale was aligned to the inflection point of a CoGa spectrum with E_0(CoGa) = E_0(Ga) = 10 367 eV. Background removal was done with the AutoBK code [40] with *Rbgk* = 1.0 Å. Fourier transformation of the k^3-weighted EXAFS function $\chi(k)$ was done with a Kaiser-Bessel window function in a *k*-range from 2.6 to 12.5 Å^{-1}.

3.2.1. *In situ spectra during the ammonolysis of β-Ga_2O_3*

At all investigated temperatures, the recorded spectra during the ammonolysis of Ga_2O_3 show complete conversion to the product phase, GaN, *i.e.* the last spectrum during the ammonolysis equals the GaN standard. This behaviour was confirmed by X-ray diffraction of the product powders. As an example, Fig. 7 shows the energy calibrated and normalized spectra during the ammonolysis reaction at 1053 K. One can see a continuous development from the initial to the end condition. The resulting radial EXAFS distribution function (RDF) is shown in Fig. 8 as a function of time.

During the ammonolysis of β-Ga_2O_3 the first coordination shell in the RDF shows only slight changes, while the second peak in the RDF increases rapidly. This behaviour is due to the nature of the second coordination shell around Ga atoms in GaN and Ga_2O_3. In the nitride, there is a clearly defined second coordination shell with 12 gallium neighbors in a distance of 3.18 Å, whereas in the oxide the second shell is very diffuse, with 20 gallium neighbors in a distance range from 3.04 to 3.44 Å. Hence, the partially destructive interference in *k*-space leads to smaller amplitude in *R*-space.

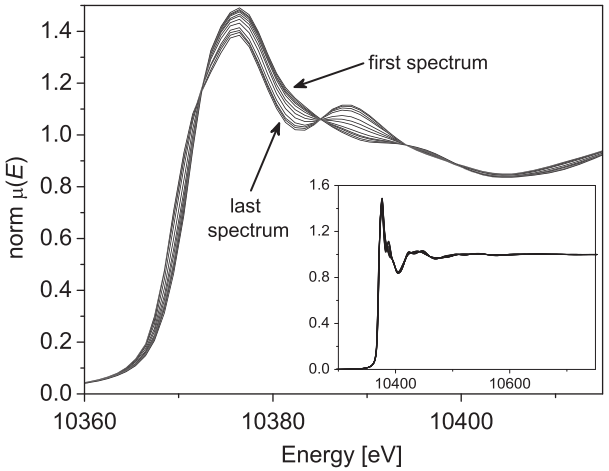

Fig. 7. Changes in the near edge region of the spectra during the ammonolysis of β-Ga_2O_3 at 1053 K. The inset shows the complete spectrum. [33] – Reproduced by permission of the PCCP Owner Societies.

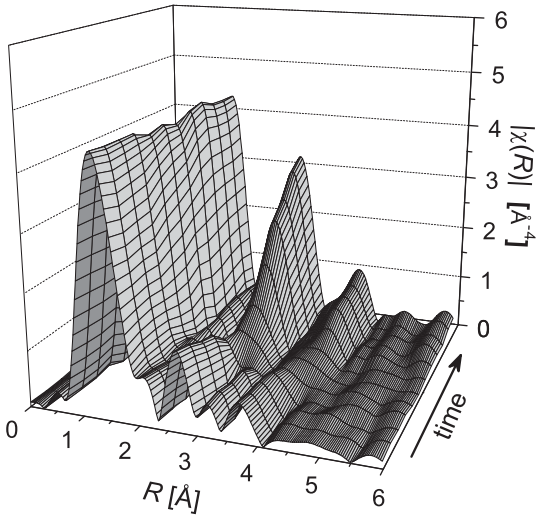

Fig. 8. Changes in the radial EXAFS distribution function (Fourier transform of k^3 $\chi(k)$) during the ammonolysis of β-Ga_2O_3 at 1053 K. [33] – Reproduced by permission of the PCCP Owner Societies.

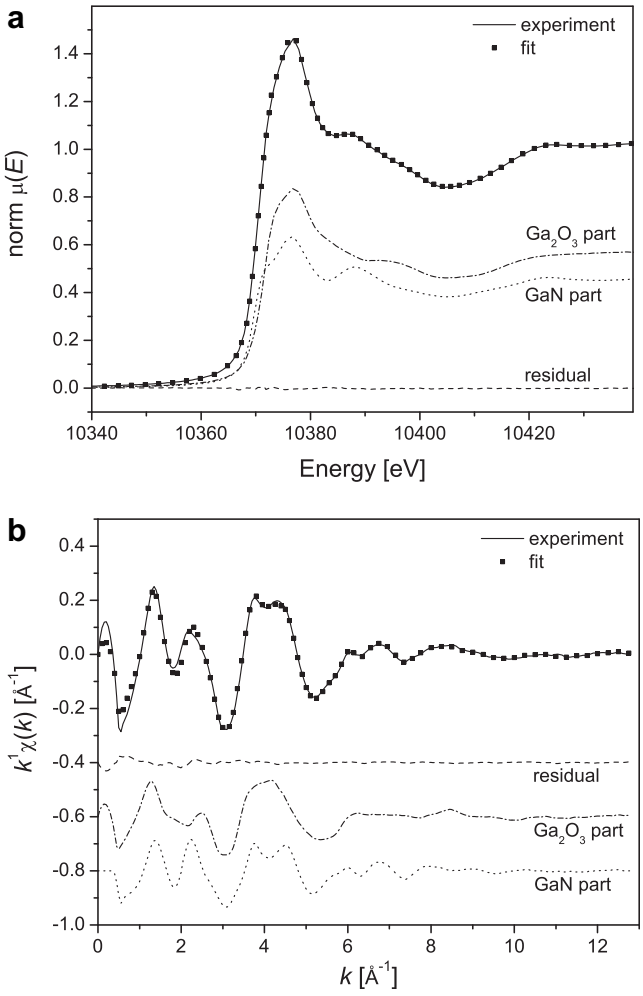

Fig. 9. Linear combination fits (dots) in *E*-space (a) and in *k*-space (b). The *in situ* spectrum (solid line) was taken during the ammonolysis of Ga_2O_3 at 1053 K after 80 min. Also shown are the contributions of the reference spectra of Ga_2O_3 and GaN and the residuals. [33] – Reproduced by permission of the PCCP Owner Societies.

3.2.2. Reaction kinetics: experiment and modeling

For a quantitative analysis of the reaction kinetics shown in Figs. 7 and 8, the normalized, time-dependent *in situ* spectra, $\mu(E,t)$, and the extracted time-dependent $\chi(k,t)$ are fitted according to Equations (1) and (2) with a linear combination of GaN and Ga_2O_3 reference spectra.

$$\mu(E,t) = a_\mu(t)\cdot\mu(E)_{Ga_2O_3} + b_\mu(t)\cdot\mu(E)_{GaN} \quad (1)$$

$$\chi(k,t) = a_\chi(t)\cdot\chi(k)_{Ga_2O_3} + b_\chi(t)\cdot\chi(k)_{GaN} \quad (2)$$

Here $\mu(E)_i$ and $\chi(k)_i$ ($i = Ga_3O_3$, GaN) are the normalized spectra (in *E*- and *k*-space) of pure β-Ga_2O_3 and α-GaN. The weighting factors $a_\mu(t)$, $b_\mu(t)$, $a_\chi(t)$, and $b_\chi(t)$ are time-dependent and describe the reaction kinetics. We fit $\mu(E,t)$ and $\chi(k,t)$ separately for the following reason. For $\mu(E,t)$, the fitting range in energy space is from 20 eV before the edge to 50 eV behind the edge. This presents a fit of the XANES-region which is sensitive to changes in the electronic structure of the samples. For $\chi(k,t)$, the fits in *k*-space are done in a fitting range from 2.5 to 9.0 $Å^{-1}$. This presents an EXAFS fit, which is sensitive to structural changes during the reaction.

In Fig. 9a, one particular *in situ* spectrum is shown, which corresponds to $t = 80$ min in the time series in Fig. 7. Also shown are the fit according to Equation (1) and the contributions of the reference spectra of Ga_2O_3 and GaN to the fit. The fit describes the experimental data well, with a small residual over the whole fitting range which shows no structure. Thus, the XANES-region reflecting the electronic structure at this particular time during the ammonolysis reaction can be described very well by a linear combination of GaN and Ga_2O_3 spectra only.

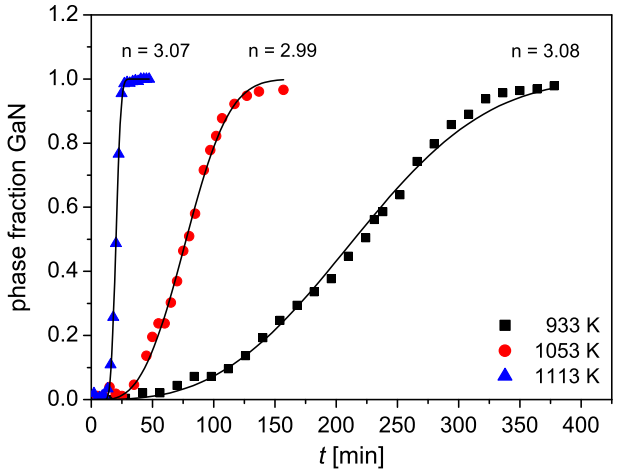

Fig. 10. Phase fraction of the product GaN during the ammonolysis of Ga_2O_3 (symbols) for three different temperatures as obtained by linear combination fitting of the *in situ* X-ray absorption spectra. The solid lines are the fits with the JMAK Equation (3). [33] – Adapted by permission of the PCCP Owner Societies.

Fig. 9b shows the corresponding fit in *k*-space. Again, the fit is in very good agreement with the experimental curve. Thus, the EXAFS-region reflecting the local structure around gallium atoms at this particular time during the ammonolysis reaction can also be described by a linear combination of GaN and Ga_2O_3 spectra only. In order to further elucidate the presence of reaction intermediates or other spectral compounds not explained by the reference spectra, the residual in Fig. 9b was Fourier transformed, just like a regular $\chi(k)$ function. However, no noticeable EXAFS RDF-like features were detected in the residual. In addition, neither a systematic time dependence of the residuals nor a correlation between residuals at consecutive time steps was found which clearly indicates that the residuals are only due to noise.

Similar results were obtained for all spectra that were taken during the ammonolysis of Ga_2O_3. At all points in time, both the electronic structure (XANES) as well as the local structure around Ga atoms (EXAFS) is in excellent agreement with the respective linear combination of the references according to Equations (1) and (2). This leads to the conclusion that no other phases than GaN and Ga_2O_3 are present during the ammonolysis reaction (within our detection limit for a new phase being in the percent range).

Table 5
Estimated incubation times t_0 for the ammonolysis of Ga_2O_3 and fit parameters *k* and *n* obtained from the fits using the extended JMAK Equation (3).

Temperature [K]	t_0 [min]	k [min^{-1}]	n	Reactant
933	0	0.0041 ± 0.0002	3.08 ± 0.07	com
1053	7	0.0122 ± 0.0003	2.99 ± 0.05	com
1053	4	0.0115 ± 0.0002	3.34 ± 0.11	com
1053	0	0.0101 ± 0.0001	3.09 ± 0.09	com
1053	0	0.0119 ± 0.0006	2.81 ± 0.09	syn
1113	11	0.1028 ± 0.0007	3.07 ± 0.12	com
1113	11	0.0701 ± 0.0005	3.44 ± 0.15	com
1113	9	0.0719 ± 0.0007	2.90 ± 0.12	syn

com: Commercial Ga_2O_3; syn: Ga_2O_3 synthesized by oxidation of GaN.

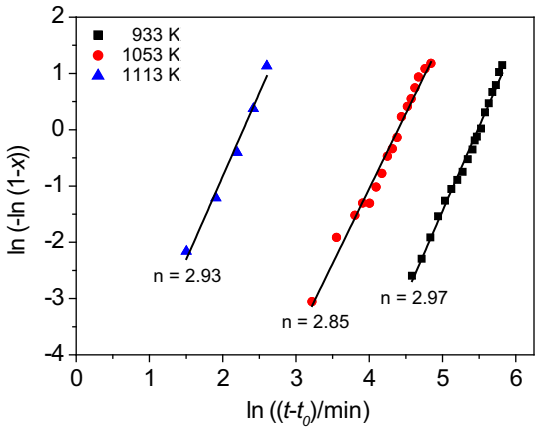

Fig. 11. Sharp–Hancock plot of the phase fraction $x(t)$ of GaN during the ammonolysis of Ga_2O_3 at different temperatures. In this presentation the Avrami exponent n is the slope of the curve. [33] – Adapted by permission of the PCCP Owner Societies.

Another important point comes out by normalizing the sum of the weighting factors $a_\mu(t)$ and $b_\mu(t)$ respectively $a_\chi(t)$ and $b_\chi(t)$ to one and comparing the remaining independent factors $b_\mu^{norm}(t)$ (from the fits in E-space) and $b_\chi^{norm}(t)$ (from the fits in k-space). We find that at all reaction temperatures and over the whole reaction time $b_\mu^{norm}(t)$ is equal to $b_\chi^{norm}(t)$. This means that the changes in the electronic structure (XANES-region) and in the short range order around Ga (EXAFS-region) proceed with the same rate. Thus, hereafter we will use only $b(t) = 1 - a(t)$ $(=b_\mu^{norm}(t) = b_\chi^{norm}(t))$ to derive the reaction kinetics.

Fig. 10 shows the phase fraction $b(t)$ of the product GaN during the ammonolysis of Ga_2O_3 as a function of the reaction time. At the beginning of the reaction, there is an incubation time during which the phase fraction of GaN does not change. After this incubation time the reaction rate increases rapidly, reaches a maximum (inflection point of the graph), and then becomes smaller again.

The shape of the kinetic graphs of the ammonolysis in Fig. 10 is typical for the well-known Johnson–Mehl–Avrami–Kolmogorow kinetics that is used to describe crystallization processes, other phase transitions and also solid state reactions with a reaction front [41–43]. Here, the phase fraction $x(t)$ of the newly formed phase as a function of time t is given by the Johnson–Mehl–Avrami–Kolmogorow equation (JMAK equation):

$$x(t) = 1 - \exp(-(k\cdot(t - t_0))^n) \quad (3)$$

Here k is the rate constant of the reaction, and n is the Avrami exponent that gives a hint on the nature of the reaction mechanism and the reaction kinetics [44]. As additional parameter we introduced the incubation time t_0 as the conversion of Ga_2O_3 to GaN shows an induction period at the beginning of the reaction (see Fig. 10). The JMAK model, on the other hand, includes only the mechanistic steps of nucleation and growth of the nuclei, and any step before nucleation (e.g. bulk or grain boundary diffusion) is not considered in the JMAK Equation (3). The incubation time is not a fit parameter, but is estimated from the graphs in Fig. 10 as the time until which there is no noticeable conversion. With Equation (3) the experimental curves in Fig. 10 can be fitted with k and n as fitting parameters. Typical fits are shown in Fig. 10 (solid lines). In all cases the experimental data are well described by the JMAK equation. The estimated incubation times t_0 and all fitting results for k and n are shown in Table 5.

To check whether the reaction proceeds by a single reaction mechanism over the whole reaction time we plotted $\ln(-\ln(1 - x(t)))$ against $\ln(t - t_0)$ in the so-called Sharp–Hancock plot [45]. The constant slopes in Fig. 11 indicate that there is no change in the reaction mechanism and the rate determining step during the whole reaction time. In addition, the slopes – reflecting the Avrami exponents n – are approximately identical at the three investigated temperatures, indicating that the reaction mechanism does not change with temperature.

The obtained Avrami exponents in Table 5 and in Fig. 11 scatter around $n = 3$. This value corresponds to a reaction mechanism with fast nucleation at the beginning of the reaction and subsequent three-dimensional growth of nuclei with a constant growth rate [44]. During the latter part of the reaction the formation of the new phase at the interface between the matrix and the nucleus is rate determining. Thus, our experimental data show that the ammonolysis of Ga_2O_3 starts with a fast nucleation of GaN nuclei and then the reaction is determined by further growth of GaN at the interface between Ga_2O_3 and GaN.

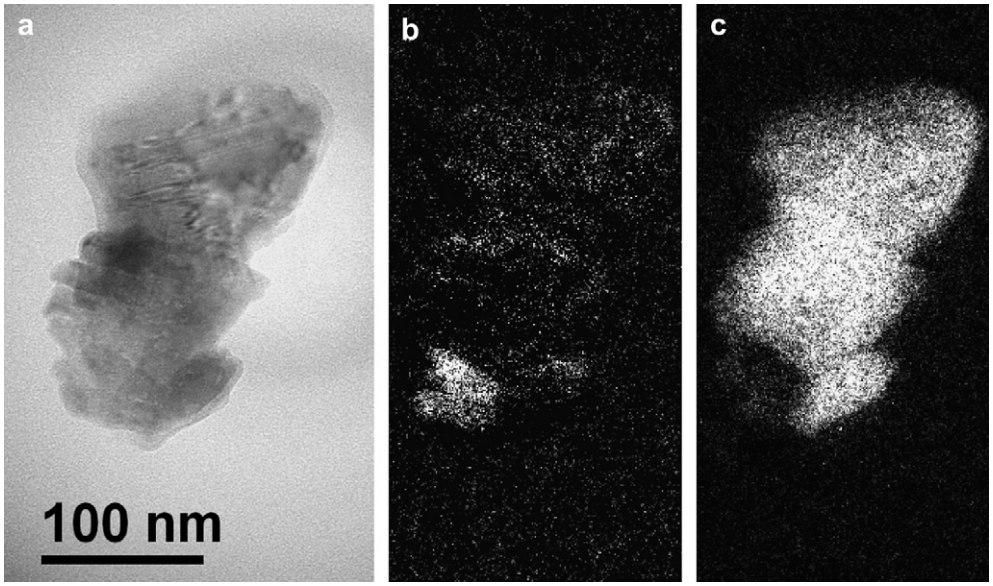

Fig. 12. Conventional TEM bright field image of a ground Ga_2O_3 particle after partial ammonolysis (a) and corresponding EFTEM element distribution maps for nitrogen (b) and oxygen (c), respectively. [33] – Reproduced by permission of the PCCP Owner Societies.

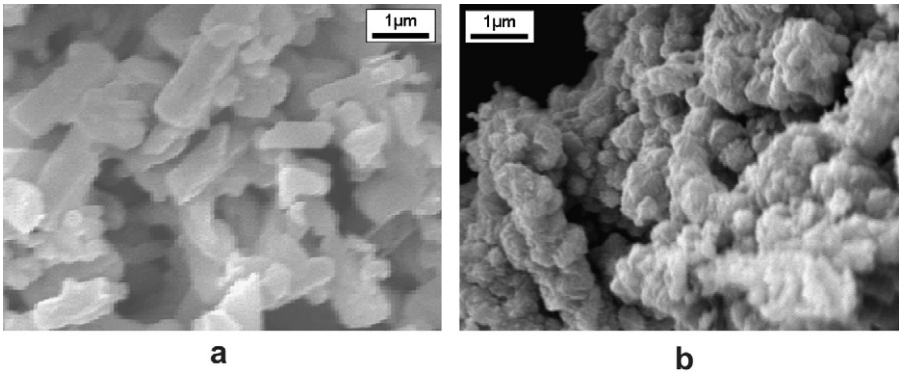

Fig. 13. SEM micrographs of the Ga_2O_3 reactant (a) and GaN product (b). [33] – Reproduced by permission of the PCCP Owner Societies.

3.3. TEM and SEM characterization

To verify the existence of GaN nuclei in the bulk or at the surface of Ga_2O_3 grains, Ga_2O_3 powder that was ammonolyzed for 60 min at 1053 K (ca. 20% conversion, see Fig. 10) was ground and analyzed by TEM. The distribution of oxygen and nitrogen within individual particles was analyzed by means of energy-filtering TEM (EFTEM) [46] using the oxygen and nitrogen *K*-edges (see Fig. 12).

A typical ground powder particle of relatively uniform thickness is shown in the TEM bright field image in Fig. 12a. The signal in the EFTEM element distribution map in Fig. 12b proves the inhomogeneous distribution of nitrogen within the investigated grain and indicates a small GaN nucleus of about 40 nm diameter at the lower left side of the particle (area of high signal). The corresponding oxygen distribution map in Fig. 12c shows that the remaining part of the particle virtually consists only of Ga_2O_3.

Another interesting point comes out by examining SEM micrographs of the Ga_2O_3 reactant and the GaN product. Fig. 13 shows that the reactant particles have block-shaped geometry. During the ammonolysis reaction these grains are totally destroyed. The GaN product has a foam-like shape and one cannot identify individual grains. A possible explanation is that the formation of the inner GaN phase produces stress in the Ga_2O_3 bulk due to the different molar volumes of Ga_2O_3 and GaN. After a certain reaction time the increasing stress results in destruction of the original grains.

We also investigated the oxidation of GaN powder to Ga_2O_3 by means of *in situ* XAS [33]. The kinetics of this reaction shows, however, a completely different behaviour compared to the ammonolysis. There is no induction period, i.e. the conversion of GaN to Ga_2O_3 starts immediately, with the maximum reaction rate at the beginning of the reaction. We modeled this kinetics using a layer growth model which was applied by Wolter et al. [47] to explain the oxidation of GaN epilayers. In our case – oxidation of GaN grains - the reaction front moves from the surface of the GaN grains into the interior, i.e. the remaining GaN grain is covered by a Ga_2O_3 layer, leaving the grain morphology unchanged. The rate determining step is the formation of the newly formed gallium oxide product phase at the interface Ga_2O_3/GaN. As the area of this interface decreases with time the reaction rate is maximal at the beginning of the reaction and then decreases, as observed experimentally.

A schematic comparison of the different reaction mechanisms for the ammonolysis of Ga_2O_3 and the oxidation of GaN is shown in Fig. 14. The ammonolysis of Ga_2O_3 is characterized by nucleation and growth of GaN nuclei resulting in destruction of the original grain morphology. In contrast, the oxidation of GaN is characterized by growth of a Ga_2O_3 layer covering the complete GaN grain and preserving the original grain morphology. In both cases, transport of nitrogen and oxygen is assumed to take place along fast diffusion pathways, such as grain boundaries or dislocations as indicated schematically in Fig. 14.

The above experimental results are supported by considering the chemical driving forces $\Delta_R G$ for both reactions [33] which are extremely different, $\Delta_R G(\text{oxidation}) \sim 25 \cdot \Delta_R G(\text{ammonolysis})$. As a consequence, the ammonolysis reaction is characterized by a small nucleation rate resulting in a few, relatively large nuclei – as observed experimentally. In contrast, the oxidation reaction is characterized by a high nucleation rate resulting in many, relatively small nuclei which – after coalescence – form a closed oxide layer, as found experimentally.

4. Spinel-type and nitrogen-rich gallium oxynitrides

In view of the chemical similarity of the earth metals aluminum and gallium, the existence of spinel-type aluminum oxynitrides, termed γ-alons, with a wide solid solution range [48] suggests that

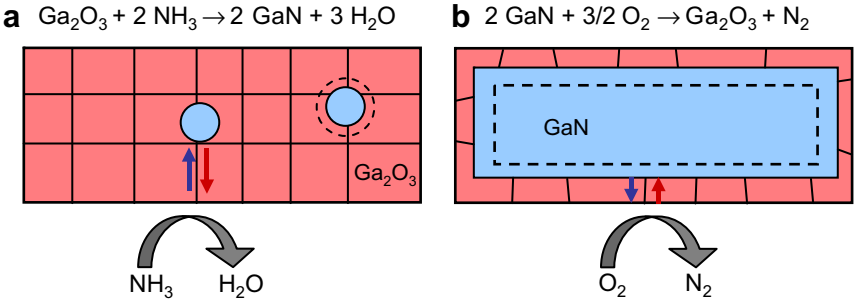

Fig. 14. Schematics of the ammonolysis of Ga_2O_3 with nucleation and growth of GaN (a) and the oxidation of GaN with growth of a Ga_2O_3 layer (b). In both cases the black lines indicate fast diffusion pathways for oxygen (red arrow) and nitrogen (blue arrow) which could be cracks, grain boundaries or dislocations. (For interpretation of the references to color in this figure legend, the reader is referred to the web version of this article.)

Table 6
Calculated crystallographic data of γ-Ga_3O_3N. The structural parameters are obtained within the GGA.

γ-Ga_3O_3N; space group R3m (166), $Z = 2$; $a = 5.9212$ Å, $\alpha = 59.26°$				
Atom	Wyckoff pos.	x	y	z
Ga1	1b	½	½	½
Ga2	3e	0	½	½
Ga3	2c	0.1368	0.1368	0.1368
N	2c	0.2669	0.2669	0.2669
O	6h	0.2599	0.2599	0.7378

similar gallium oxynitrides, γ-galons, may exist too. Puchinger et al. [49] postulated a gallium oxynitride with spinel-type structure based on observed diffraction ring patterns and high-resolution transmission electron microscopy (HRTEM) plane spacings. Kroll et al. [50] then investigated the stability of these compounds using density-functional theory and Kroll [51] could show that γ-galons are only stable at elevated pressures. Shortly after, Soignard et al. [52] and Kinski et al. [53] could synthesize defective spinels at pressures of several GPa and elevated temperatures of 2000 K and 1300 K, respectively. In Sections 4.1 and 4.2 we summarize theoretical results on the stability of γ-galons [50].

Nitrogen-rich gallium oxynitrides that are derived from wurtzite-type GaN are known since a while (see [6–13]). In Section 4.3 theoretical results on the stability and structure of Cr- and Fe-doped oxynitrides are summarized.

4.1. Spinel-type gallium oxynitride, Ga_3O_3N

To calculate possible approximants of spinel-type γ-Ga_3O_3N we followed the tracks outlined by Fang et al. in their investigation [54] of spinel-type compounds of aluminum oxynitride. We first chose a model denoted γ-Ga_3O_3N, in which Ga atoms fill all cation positions of the spinel structure, both the tetrahedrally coordinated and the octahedrally coordinated sites [50]. The anion sublattice, a slightly distorted ccp arrangement, is made up by both N and O, in quantities of ¼ and ¾ of all available 32 anion positions, respectively. Note that a true mixture within the anion sublattice will give a substantial contribution to configurational entropy. In our calculation we are bound to compute structures with full occupation of every site, and non-integer occupations are usually treated within a supercell approach. Therefore, we set out and computed several possible structures of spinel-type γ-Ga_3O_3N, all with 56 atoms in the unit cell. We started with a model isostructural to the suggestion made for γ-Al_3O_3N by Fang et al. but extended the search to various patterns for the N/O distribution. Through this procedure we not only established the lowest energy polymorph, which turned out to be isostructural to the lowest energy structure of γ-Al_3O_3N, but also accessed the differences in energy between the different patterns. Hence, by means of our computational approach we developed an understanding of the effects governing such energy differences. The lowest energy structure of γ-Ga_3O_3N is characterized by a regular distribution of N atoms, forming a (distorted) simple cubic substructure within the anion sublattice. Hence, the formally charged N^{3-} anions maximize their distance. The second-nearest neighbor shell (the anion–anion coordination) of N is composed of 12 oxygen atoms, while that of O comprises four nitrogen and 8 oxygen atoms. The spinel structure then comprises twice as much octahedrally as tetrahedrally coordinated Ga atoms. Of the Ga atoms in octahedral sites, a quarter (Wyckoff position 1*b*) are coordinated by O only, forming {Ga}O_6 octahedra. The remaining three quarters (in 3*e*) have two nitrogen (in trans position) and four oxygen nearest neighbors, {Ga}N_2O_4. Each of the tetrahedral Ga (in 2*c*) has three oxygen nearest neighbors and one nitrogen nearest neighbor, {Ga}NO_3. The structure adopts rhombohedral symmetry, R3m, and can easily be described using a unit cell that resembles the primitive unit cell of the face-centered cubic spinel structure type. The structural parameters calculated within the GGA are given in Table 6.

By relating the rhombohedral structure of Ga_3O_3N to the primitive unit cell of the face-centered cubic spinel structure it becomes obvious that the N atoms in the rhombohedral approximant form two independent distorted face-centered sublattices. We can generate two more approximants of γ-Ga_3O_3N with rhombohedral symmetry that exhibit this particular feature. They are, however, unfavorable in energy by 0.12 eV and 0.24 eV per Ga_3O_3N, respectively. To investigate preferential bonding we constructed two more models with 56 atoms in the unit cell. One comprises {Ga}N_4-tetrahedra, the other {Ga}N_6-octahedra, besides several other mixed O/N environments of Ga. These two approximants came out by 0.24 eV (GaN_4-tet) and 0.25 eV (GaN_6-oct) per Ga_3O_3N higher in energy than the ground state, respectively. A tetragonal approximant (space group $P4_1$) of Ga_3O_3N, with 28 atoms in the unit cell, was 0.09 eV per Ga_3O_3N higher in energy. This structure comprises {Ga}NO_3 tetrahedra, {Ga}N_2O_4-(cis) and {Ga}NO_5 octahedra. We constructed even more structures by exchanging an N atom with a nearby O atom, always using the 56-atom supercell. All these structures came out higher in energy than the lowest energy structure. The energy difference of this kind of structural defect scatters from 0.22 eV to 0.5 eV per 56 atoms. Data of two such structures are included in Table 7.

We now can compute the energy difference between Ga_3O_3N and a phase assemblage of Ga_2O_3 and GaN according to the reaction $Ga_2O_3 + GaN \rightarrow Ga_3O_3N$. Using the lowest energy structure of each composition, respectively, we estimate the enthalpy of formation of a spinel-type γ-Ga_3O_3N to be endothermic $\Delta H = +0.285$ eV per Ga_3O_3N. Using the corundum modification of Ga_2O_3 instead, the energy difference still is +0.214 eV per Ga_3O_3N. Hence, the ternary compound will not form unless it is stabilized at elevated temperatures by substantial entropy contributions ΔS. A comparison can be made readily to γ-alons with composition Al_3O_3N. We find that Al_3O_3N is less favorable by +0.256 eV (per Al_3O_3N) than a phase assemblage of corundum Al_2O_3 and AlN (+0.226 eV is the value calculated by Fang et al. [54]). Thus, were it not for the phase β-Ga_2O_3, the energetics would look at least as good as for comparable γ-alons.

Table 7
Energy relative to the lowest energy modification ($E_0 = -243.464$ eV) and volume (per formula unit) calculated for several approximants of spinel-type Ga_3O_3N (all values refer to $T = 0$ K). The labels refer to structures as described in the text.

Structure	Energy/eV	Volume/Å^3
R3m	0	72.13
O/N-exch-a	0.027	72.13
O/N-exch-b	0.062	72.13
$P4_1$	0.093	72.19
R3m-b	0.121	72.38
R3m-c	0.235	72.38
GaN_4-tet	0.242	72.30
GaN_6-oct	0.248	72.30

Table 8
Enthalpy and entropy contribution of ideal mixing at 1000 K for spinel-type gallium oxynitrides and gallia. All values are given in eV per atom, assuming a spinel unit cell with 56 sites.

γ-Galon structure	ΔH/atom	$T\cdot\Delta_{mix}S^{an}$/atom	$T\cdot\Delta_{mix}S^{cat}$/atom
Ga_3O_3N	0.041	0.0276	0
$Ga_{23}O_{27}N_5$	0.037	0.0213	0.0057
$Ga_{22}O_{30}N_2$	0.030	0.0113	0.0093
γ-Ga_2O_3	0.030	0	0.0125

4.2. Defective spinel-type structures

To model defective spinel-type gallium oxynitride structures we employed the Constant-Anion-Model [55,56]. In this model, the anion sublattice of the spinel is complete, while the cation sublattice comprises vacancies. We checked the energetics of some approximants constructed with interstitial anions (Constant-Cation-Model), but found a huge penalty for introducing an additional atom. Guided by the work of Fang et al. on γ-alons [54] we started from our lowest energy model of γ-Ga_3O_3N with rhombohedral symmetry and set it into a 56-atom supercell. We then discarded a single Ga atom from the structure. Charge balance between the cation and anion sublattices is achieved by replacing three N atoms by three O atoms. $Ga_{23}O_{27}N_5$ ($9Ga_2O_3 \cdot 5GaN$) then corresponds to 35.7 mol% GaN in the oxynitride phase, which is fairly close to the experimental value of 30 mol% [49]. There are three possibilities for the generation of a Ga vacancy, but a manifold of configurations exist on how to distribute the vacancy site as well as the anions in the model. In general, we achieve appreciable low energy structures by maximizing the distance between the N atoms as to minimize the coulomb repulsion between the (formally) N^{3-} ions. Hence, the nitrogen positions of the initial γ-Ga_3O_3N structure (Table 8 and Fig. 15) provide a good starting point for structures with either tetrahedral or octahedral Ga vacancies. The lowest energy structure of $Ga_{23}O_{27}N_5$ we found exhibits an octahedral vacancy. The structure, which is shown in Fig. 15, differs from that of the lowest energy structure of $Al_{23}O_{27}N_5$ proposed by Fang et al. [54].

Fang's defective model had N atoms deployed only from one of the two face-centered sublattices (the other remains intact), a result that we confirmed for $Al_{23}O_{27}N_5$. Our model of $Ga_{23}O_{27}N_5$ with lowest energy, however, has N atoms replaced in both face-centered sublattices. The model comprises five octahedra of the environments $\{Ga\}N_2O_4$, $\{Ga\}NO_5$, and $\{Ga\}O_6$. In addition there are three $\{Ga\}O_4$ and five $\{Ga\}NO_3$ tetrahedra. The vacant Ga site is surrounded by O only, hence exhibiting $\{V\}O_6$ octahedra, and is located in those layers of the spinel structure which are built up from both tetrahedra and octahedra (V = vacancy). We calculated the other four independent patterns for a substitution of O onto the initial sites of N of the rhombohedral Ga_3O_3N structure. The energies for all patterns are within 0.3 eV (per 55 atoms) relative to the lowest energy structure. Discarding Ga from layers which are built up from octahedral only, hence out of the $\{Ga\}N_2O_4$-octahedra, provides some structures that are comparable in energy, only 0.06 eV (per 55 atoms) higher. Here, too, we studied all independent patterns for a substitution of O with a starting geometry of N′s as in the rhombohedral Ga_3O_3N structure. The favorable structures of this type have, again, the vacancy surrounded by O only. The penalty for having an N atom adjacent to a vacancy ($\{V\}NO_5$) is at least 1.1 eV. The lowest structure with a tetrahedral vacancy in the cation sublattice then shows an excess of about 0.4 eV (per 55 atoms). We, thus, have a strong indication that in defective γ-galons vacancies are predominantly $\{V\}O_6$ octahedral vacancies. Additional tetrahedral vacancies cannot be excluded, however, because an energy difference of 0.4 eV per 55 atoms is comparable to the thermal energy of the ensemble at, say, 1000 K. The calculated lattice geometry of all defective structures is close to a rectangular cell with equal lattice parameters, reminiscent of the original cubic spinel structure. The actual symmetry of the lowest energy modification is monoclinic, and the volume of the cell is 571.4 $Å^3$ (541.1 $Å^3$ in LDA). In comparison to γ-Ga_3O_3N (GGA 577.2 $Å^3$, LDA 546.6 $Å^3$ for the 56 atoms), this is a reduction by 1%. The energetics of this phase are accessed in a similar way as for γ-Ga_3O_3N, this time we use the formation reaction $9\,Ga2O3 + 5\,GaN \rightarrow Ga_{23}O_{27}N_5$. We find an endothermic enthalpy of formation of $Ga_{23}O_{27}N_5$ of $\Delta H = +2.04$ eV per formula unit $Ga_{23}O_{27}N_5$. If we compare this enthalpy (0.037 eV per atom) with the previous value for γ-Ga_3O_3N (0.041 eV), we notice that the defective spinel phase has a lower enthalpy of formation. ΔH is still positive, however. Once again we can do the assessment with respect to the corundum modification of Ga_2O_3. This approach, of course, is more favorable in comparison to an account with respect to β-Ga_2O_3 and yields ΔH of 0.025 eV per atom. In the Al–O–N system the corresponding value comes out as $\Delta H = 0.033$ eV per atom (0.029 eV calculated by Fang et al. [54]). The outcome, thus, is essentially the same as before: if only a corundum Ga_2O_3 existed, the defective spinel modification of $Ga_{23}O_{27}N_5$ would have a lower formation energy (by 15–25%) than the corresponding γ-alon phase. The feasibility of β-Ga_2O_3 in the phase diagram, however, renders ΔH more than 10% larger than for γ-alons and makes the formation of the ternary compound less favorable.

We depleted the defective spinel $Ga_{23}O_{27}N_5$ by yet another Ga atom, yielding the composition $Ga_{22}O_{30}N_2$ ($10Ga_2O_3 \cdot 2GaN$). This corresponds to 16.7 mol% GaN in the oxynitride phase. The structure with lowest energy is also shown in Fig. 15. We calculated several approximants of this phase too, all constructed by starting with one of the more favorable models of $Ga_{23}O_{27}N_5$. Once again, we found the trend that structures with low energy are obtained by

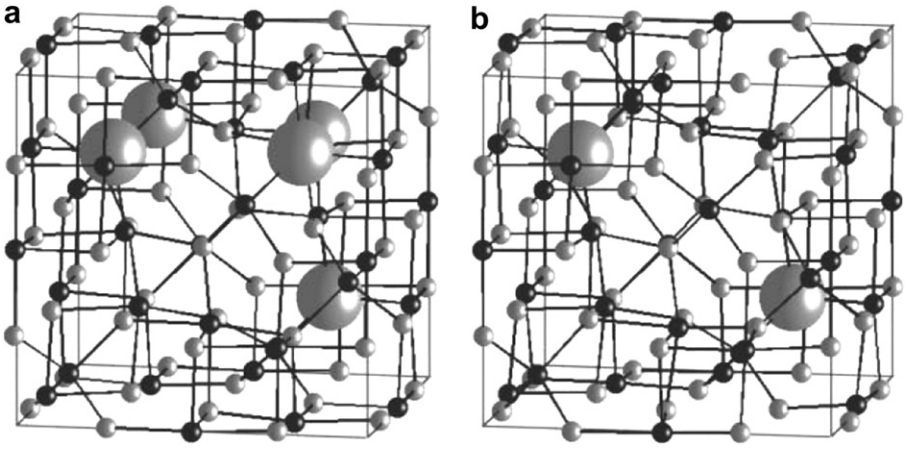

Fig. 15. Lowest energy structures of defective spinel-type structure of $Ga_{23}O_{27}N_5$ (a) and $Ga_{22}O_{30}N_2$ (b). Ga, N, and O atoms are shown as small black, large grey and small grey spheres, respectively. N atoms are emphasized in size to mark their positions. Reprinted from [50] with the kind permission of the Royal Society of Chemistry.

maximizing the distance between the remaining two N atoms in the unit cell. Furthermore, N atoms should be four-connected, not adjacent to a vacancy. The latter ones are always octahedrally surrounded by O in low energy configurations, and distributed over all available octahedral sites. No trend for defect clusters could be detected in the 56-site unit cell. The structure with lowest energy we found exhibiting one octahedral and one tetrahedral vacancy in the cation sublattice has an excess energy of about 0.3 eV (per 54 atoms). Due to the presence of two defect sites in the unit cell, the models of $Ga_{22}O_{30}N_2$ tend to exhibit lattice parameters with a larger deviation from the cubic geometry in comparison to the $Ga_{23}O_{27}N_5$ models. The energetics of this phase are accessed via the formation reaction 10 Ga_2O_3 + 2 GaN → $Ga_{22}O_{30}N_2$. The estimated enthalpy is $\Delta H = +1.6$ eV per formula unit $Ga_{22}O_{30}N_2$. This value (0.030 eV per atom) appears to be even more favorable in comparison to the values we calculated for γ-Ga_3O_3N and $Ga_{23}O_{27}N_5$.

The above results indicate that a spinel-type gallium oxynitride phase has a positive enthalpy of formation. Therefore, if we base our argument on enthalpy, which is correct for zero temperature, it looks impossible to synthesize the ternary compound using equilibrium methods. However, such a simple enthalpy assessment holds for spinel-type aluminum oxynitride as well—and both γ-alons and γ-galons are attainable through high-temperature synthesis [48,52,53]. We may attribute these favorable thermodynamics at elevated temperatures as being due to contributions of entropy differences between the solid compounds to the Gibbs energy, Δ*G*. Such entropy terms arise predominantly from a mixing of O and N within the anion sublattice as well as of vacancies within the octahedral sites of the cation sublattice. The ideal entropy of mixing, $\Delta_{mix}S$, is given by:

$$\begin{aligned}\Delta_{mix}S &= \Delta_{mix}S^{cat} + \Delta_{mix}S^{an} \\ &= R\Big[M_{cat}\left(x_{Ga[o]}\ln x_{Ga[o]} + x_{V[o]}\ln x_{V[o]}\right) + M_{an}(x_N \ln x_N \\ &\quad + x_O \ln x_O)\Big]\end{aligned} \tag{4}$$

In this equation, *R* is the universal gas constant and x_N, x_O, $x_{Ga[o]}$, and $x_{V[o]}$ are the occupation fractions of N, O, and octahedrally coordinated Ga and vacancies, respectively. M_{cat} and M_{an} are multipliers to account for the number (mol) of available sites in the unit cell. In this approach we neglect explicitly ordering effects that we employed implicitly to find the lowest energy structures. If we neglect further contributions to $\Delta_{mix}S$, the free enthalpy of formation is given by $\Delta G = \Delta H - T\Delta S_{mix}$. Inserting the proper values we obtain the results given in Table 8. For convenience we list the values in eV per atom, assuming a spinel unit cell with 56 sites. With our approach, we find that at 1000 K all spinel-type phases are not yet stable thermodynamically with respect to the binaries β-Ga_2O_3 and GaN. The temperature above which the spinel will form is 1486, 1370, 1456, and 2400 K in the order Ga_3O_3N, $Ga_{23}O_{27}N_5$, $Ga_{22}O_{30}N_2$ to γ-Ga_2O_3. Hence, defective spinel-type oxynitrides are favored over the "full" Ga_3O_3N. Nitridation of the spinel-type gallium oxide is very likely as well.

According to the results we expect spinel-type gallium oxynitrides, if they can be realized, to adopt a defective structure. This is very similar to spinel-type aluminum oxynitrides [48]. While the anion sublattice will be filled completely, the cation sublattice will exhibit octahedral vacancies. The octahedral vacancy is surrounded by oxygen atoms and favored over the tetrahedral vacancy. Nitrogen tends to reside on four-fold coordinated sites, avoiding the neighborhood of a vacancy. There is a trend of separating nitrogen ions as far as possible from each other. If we calculate the lattice parameter of a cubic γ-galon, which we derive from the volume of our non-cubic models, as a function of the GaN content, we find the trend shown in Fig. 16a. The lattice parameter depends approximately linearly on the phase content of GaN, with larger parameter for higher GaN content. The experimental lattice parameter of Puchinger et al. [49] fits very well into the diagram, accepting that typical GGA and LDA calculations over- and underestimate, respectively, such structural quantities. A defective spinel-type γ-galon with less than 50 mol% GaN will be favored energetically over the "filled" γ-Ga_3O_3N. Nevertheless, the enthalpy of formation of all γ-galons is positive, indicating that a phase assemblage of oxide (β-Ga_2O_3) and nitride (GaN) is more stable than oxynitride (γ-galon). This effect is significantly more pronounced than in comparable aluminum oxynitrides, so-called γ-alons. We traced the increased difficulties to be directly related to the ground state modification of monoclinic β-Ga_2O_3, which comes out lower in energy than a corundum-type α-Ga_2O_3. Formation of the ternary phase, thus, needs to go along with substantial contributions of configurational entropy arising from the disorder of oxygen and nitrogen within the anion sublattice. As we have shown, a temperature of some 1300–1500 K will at least be needed to balance the formation reaction, if we base our arguments on an ideal mixture of O and N. This temperature is rather close to or even beyond the thermal stability of GaN (1000–1400 K [57,58], making it rather difficult to synthesize the ternary phase from a mixture of Ga_2O_3 and GaN.

While the above calculations were done for ambient pressure conditions, Kroll [51] could demonstrate that the formation enthalpy of galons decreases with increasing pressure and reaches a minimum at the $\beta \rightarrow \alpha$ phase transformation of gallium oxide. Thus, Kroll proposed to synthesize gallons at pressures of 2–6 GPa and temperatures of about 2000 K which corresponds roughly to

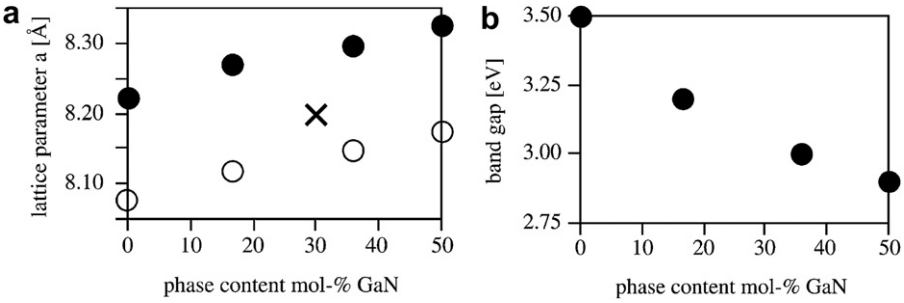

Fig. 16. Left: lattice parameter of a "cubic" spinel-type γ-galon as a function of the GaN content. Full circles refer to GGA calculations, open circles to LDA calculations. The cross denotes the experimental data determined by Puchinger et al. [49]. Right: band gap calculated within the GGA of spinel-type γ-galons and γ-Ga_2O_3 as a function of the GaN content. Reprinted from [50] with the kind permission of the Royal Society of Chemistry.

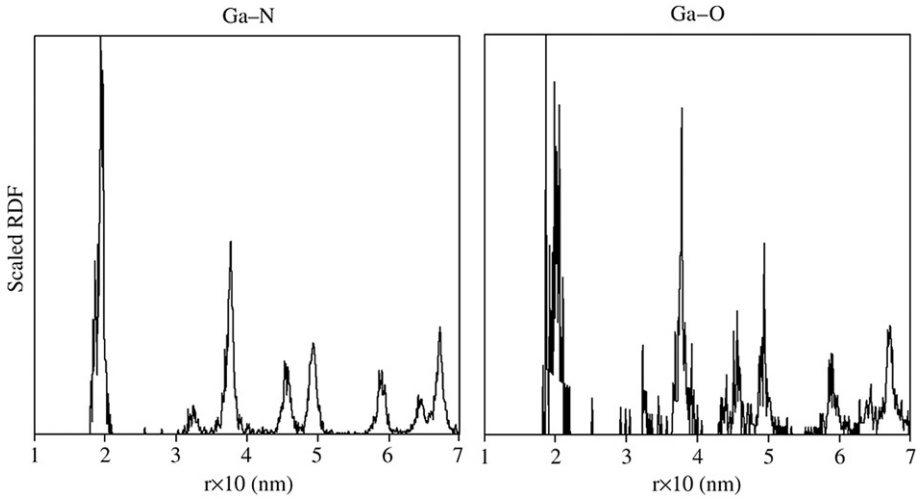

Fig. 17. Scaled radial distribution around Ga for gallium oxynitride doped with 1 at.% chromium on the basis of *ab-initio* electronic structure theory. Reprinted from [59] with the kind permission of Elsevier.

the experimental conditions of the syntheses reported by Soignard et al. [52] and Kinski et al. [53].

Galons offer the potential for engineering the band gap of the material. Experimental values of the optical band gap for wurtzite GaN and β-Ga_2O_3 are 3.5 eV and 4.9 eV, respectively [27,18]. In Fig. 16b the calculated band gap of γ-Ga_3O_3N is displayed as a function of GaN content. Though density-functional calculations typically underestimate the true gap of a material (by some 20–50%), the data exhibit a variation of approximately 20% from 2.9 eV in γ-Ga_3O_3N to 3.5 eV in γ-Ga_2O_3.

4.3. Doped, nitrogen-rich gallium oxynitrides

Chromium-doped, nitrogen-rich gallium oxynitrides crystallizing in the Wurtzite structure and having a chemical composition $\{(Ga_{0.99}Cr_{0.01})_{0.90}V_{0.10}\}(N_{0.69}O_{0.31})$ (V = cation vacancy) were prepared by ammonia nitridation of oxide precursors derived via the citrate route. The solid solution limits of less than 1 at.% Cr^{3+} were confirmed by both XRD and EXAFS on the nitrided product at 1023 K in the wurtzite-type crystal lattice [59]. The precursors were X-ray amorphous. The nitrided product without Cr doping was a nitrogen-rich gallium oxynitride as previously reported [60]. It had a wurtzite lattice with $a = 0.3189(7)$ nm and $c = 0.5182(12)$ nm. If it is prepared at 1123 K, the lattice parameters were reduced to $a = 0.3187(4)$ nm, $c = 0.5180(9)$ nm and the crystallinity was improved. The lattice parameters obtained by the density-functional total energy calculations yielded $a = 0.317(8)$ nm, $c = 0.510(14)$ nm and $\gamma = 121.61(1)$. Within the uncertainty range, theory and experiment are in excellent agreement.

To get insight into the structure of the Cr-doped gallium oxynitrides, the radial distribution functions were calculated starting from the quantum-chemical model for the ca. 1 at.% chromium-doped product. Figs. 17 and 18 present the theoretical radial distributions around gallium and chromium in the electronically as well as structurally relaxed supercell. The nearest neighbors are about 0.20 nm away for Ga – *X* and, somewhat less, about 0.18 nm, for Cr – *X*. The structural optimization within the density-functional framework clearly indicates that Cr^{3+} is substituting Ga^{3+} in the gallium oxynitride crystal lattice, and the tetrahedral coordination of Cr^{3+} is a local minimum on the energy landscape. Owing to the cation vacancies within the lattice, the surrounding anions shift slightly away from their ideal positions, and this results in slightly broader profiles for the radial distribution functions than in an ideal ionic lattice.

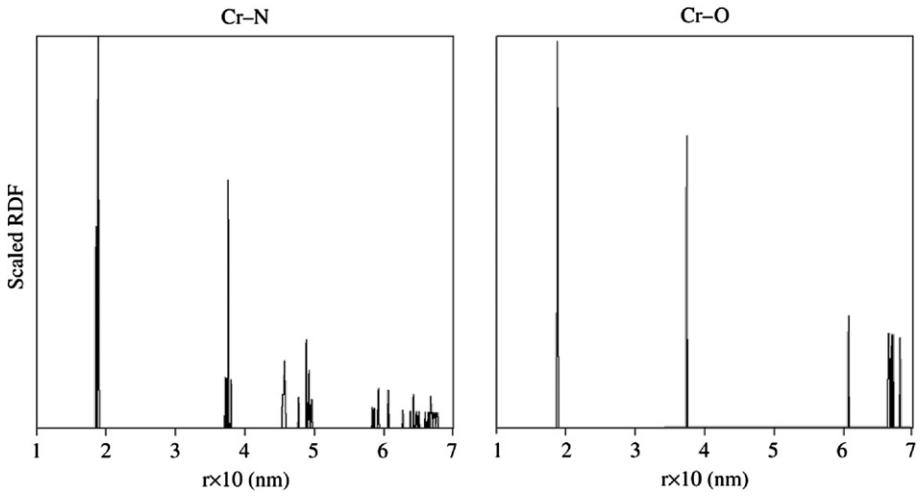

Fig. 18. Scaled radial distribution around Cr for gallium oxynitride doped with 1 at.% chromium on the basis of *ab-initio* electronic structure theory. Reprinted from [59] with the kind permission of Elsevier.

The magnetic properties of the gallium oxynitride doped with 1 at.% Cr prepared at 1023 K were also investigated. The field dependence showed a weak magnetic interaction at 5 K. Its temperature dependence revealed almost paramagnetic behaviour. The magnetic susceptibility increased very slightly above 100 K, probably due to the antiferromagnetic CrN impurity with $T_N = 285$ K. There was no magnetic interaction between the dopant Cr^{3+} ions in the gallium oxynitride host for very small amounts of Cr^{3+}. To gain further insight into the magnetic attributes of the material, we also performed spin-polarized GGA calculations of gallium oxynitride doped with 1 at.% Cr. It was found that the total energies are lowered by merely about 0.06 eV, simply due to the slightly different occupations of the α and β spin sublattices. The magnetic moment is located solely on the chromium atom, and there is no indication of long-range magnetic order. This is not surprising since itinerant electrons are missing and, also, for such a small doping, the average Cr^{3+}–Cr^{3+} distance reaches more than 1.4 nm, thereby excluding significant interatomic overlap. This is consistent with the weak magnetic interaction observed experimentally.

In summary, gallium oxynitride prepared via the solution route could be doped by trivalent chromium only up to 1 at.%. The solid solution limit was narrow in comparison to the 10 at.% for the doping of Mn^{2+} [61] and Li^{+} [60], probably because Cr^{3+} ions normally occupy octahedral sites, rather than tetrahedral Ga^{3+} sites in the wurtzite-type crystal lattice [62]. *Ab-initio* electronic structure calculations confirm the metastable nature of the oxynitride material, and demonstrate that spin-polarized Cr^{3+} replaces Ga^{3+} in its tetrahedral site [59].

Besides the chromium-doped oxynitrides also iron-doped gallium oxynitrides with similar compositions were investigated [63]. Here we focused on possible ordering effects of the cations as well as the anions. DFT calculations were used to investigate the distribution of cations and anions within Fe-doped hexagonal gallium oxynitride. One example of such a Fe-O-cluster inside the wurtzite lattice of gallium oxynitride is shown in Fig. 19.

In good agreement with the experimental results, the Fe-O-clustered systems are always energetically preferred over the other atomic distributions. The calculated total energies for these systems are about 5–8 eV/unit cell lower in energy than the other distributions because the iron cations clearly prefer to surround themselves by a nearest-neighbors oxygen shell.

5. Amorphous, non-stoichiometric gallium oxide

In contrast to the previous sections, we consider now non-stoichiometric gallium oxides with large gallium excess (or oxygen deficit) which are located aside stoichiometric β-Ga_2O_3 and the quasi-binary line connecting Ga_2O_3 and GaN (see Fig. 1). We prepared these metastable materials by means of pulsed laser deposition (PLD) and found that the as-prepared oxides are amorphous. These new materials show an unprecedented insulator–metal transition, with a jump in conductivity of ca. 7 orders of magnitude at temperatures as high as 670 K [64]. We could show that this insulator–metal transition is chemically induced by an internal redox reaction (a disproportionation), namely the crystallization of stoichiometric β-Ga_2O_3 within the amorphous oxide matrix, which becomes as a result even more non-stoichiometric. That is, a solid state reaction drives the insulator–metal transition. This phenomenon is rather surprising as gallium is a main group element, while most insulator–metal transitions are known for transition metal compounds [65,66]. Subsequently, we will summarize the results published in Ref. [64].

5.1. Experimental

The Pulsed Laser Deposition technique has been employed for the deposition of films of gallium oxide. Laser ablation and subsequent deposition is a versatile technique to grow epitaxial films and multilayers in various gaseous atmospheres [67]. Gallium oxide films were deposited on heated polycrystalline and single crystalline sapphire substrates with (0001) orientation. Pellets of Ga_2O_3 were prepared as target materials by pelletizing Ga_2O_3 powder (Alfa Aeser, 99.999%) and subsequently sintering them at 1573 K. A KrF excimer laser pulse ($\lambda = 248$ nm, $\tau = 10$ ns) (Lambda Physik, Germany) with energy of 200 mJ was used for the ablation of the Ga_2O_3 targets. The laser evaporated species were deposited onto the substrates kept at a distance of ~4 cm from the target surface. The deposition was carried out for 45 min and the substrate temperature was maintained at 873 K. Films were deposited in

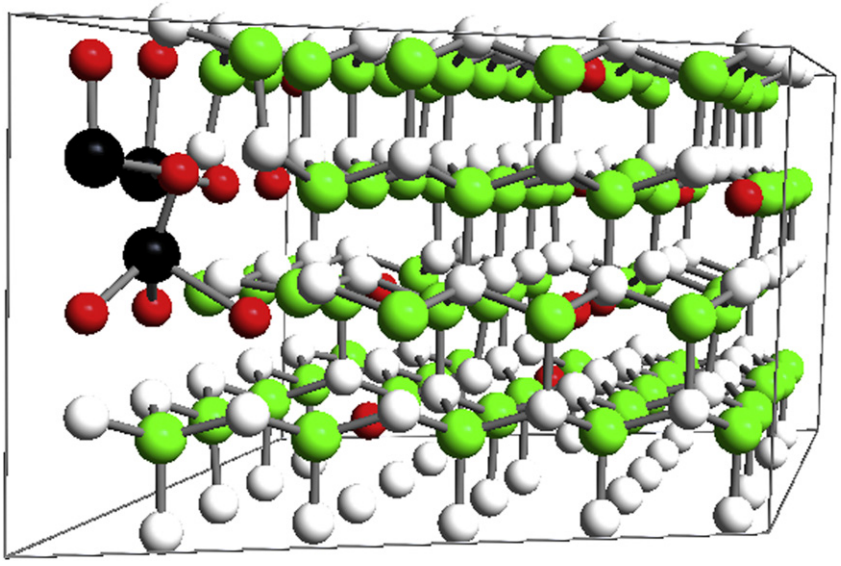

Fig. 19. Computational model of gallium oxynitride in the hexagonal wurtzite structure doped with a Fe-O-cluster. The iron atoms are in black, oxygen is red, nitrogen is colored green and gallium is white. Reprinted from [63] with the kind permission of Elsevier. (For interpretation of the references to color in this figure legend, the reader is referred to the web version of this article.)

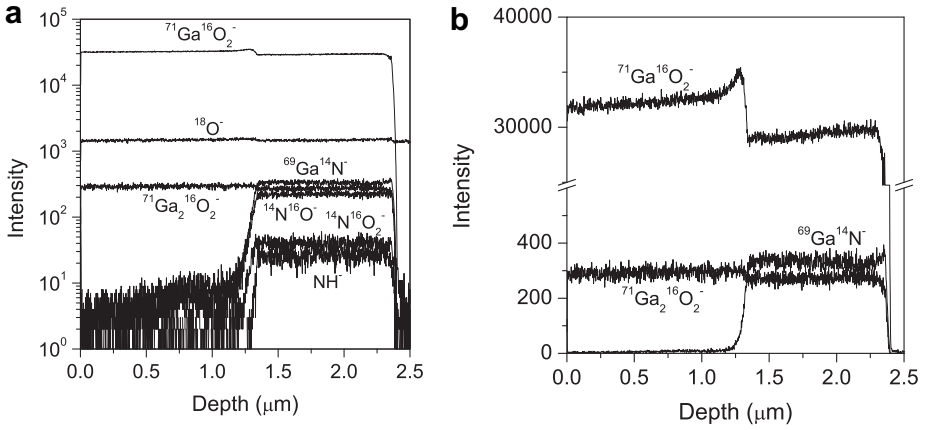

Fig. 20. (a) SIMS depth profile of a $Ga_2O_3(O_2)/Ga_2O_3(N_2)$ double layer deposited on a single crystalline Al_2O_3 substrate shown in a logarithmic intensity scale. (b) SIMS depth profiles of $^{71}Ga_2^{16}O_2^-$, $^{71}Ga^{16}O_2^-$ and $^{69}Ga^{14}N^-$ in the $Ga_2O_3(O_2)/Ga_2O_3(N_2)$ double layer shown on a linear intensity scale.

atmospheres of oxygen, nitrogen or argon, with pressures varying from 0.02 to 0.08 mbar.

The surface morphology of the films was examined with interference microscopy (NT 1100, Veeco Instruments), and the chemical composition of the films was analyzed by means of Electron Probe Micro Analysis (EPMA) with a CAMEBAX SX 50 (Cameca, France) instrument. Also Secondary Ion Mass Spectrometry (SIMS) was employed to detect the presence of nitrogen in the deposited gallium oxide layer. Depth profiling was performed with a dual beam TOF-SIMS IV (IONTOF GmbH, Germany) instrument. It is noted that N^- is unstable with respect to $N + e^-$ and is therefore unsuitable for SIMS analysis of nitrogen. Instead, the intensities of negative molecular secondary ions containing N were monitored, the approach usually taken in the literature [68]. The parallel detection capability of TOF-SIMS permitted the monitoring of a large number of secondary ions without any loss of data density. The crater depths were determined post analysis by interference microscopy.

The electrical conductivity of the films was measured in an in-house van der Pauw setup for temperatures between RT and 973 K and a Quantum Design PPMS (Quantum Design, USA) for temperatures between 5 K and RT.

X-ray absorption spectroscopy was performed on the films using the experimental techniques that were described in detail in Section 3.2.

In situ X-ray diffraction studies have been carried out in a STOE theta-theta diffractometer with Co Kα radiation ($\lambda = 1.7902$ Å). The diffractometer is equipped with a high temperature chamber (HDK 2.4K, Johanna Otto GmbH) employing a Pt–Rh heating element. Temperature resolved X-ray diffraction patterns were recorded with a linear position sensitive detector.

In situ optical absorption spectra of the films deposited on Al_2O_3 substrates were recorded at elevated temperatures in a Perkin Elmer (Lambda 900) Spectrophotometer in the 250–860 nm wavelength region.

5.2. Chemical characterization

We prepared films with thicknesses between 1 and 6 μm. Films prepared in pure oxygen were deposited stoichiometrically, i.e. with a composition Ga:O of 0.40:0.60 as expected for Ga_2O_3. In contrast, the films deposited under reducing conditions (pure nitrogen or pure argon atmosphere) are highly non-stoichiometric with typical compositions Ga:O of 0.45:0.55 (argon) or Ga:O:N of

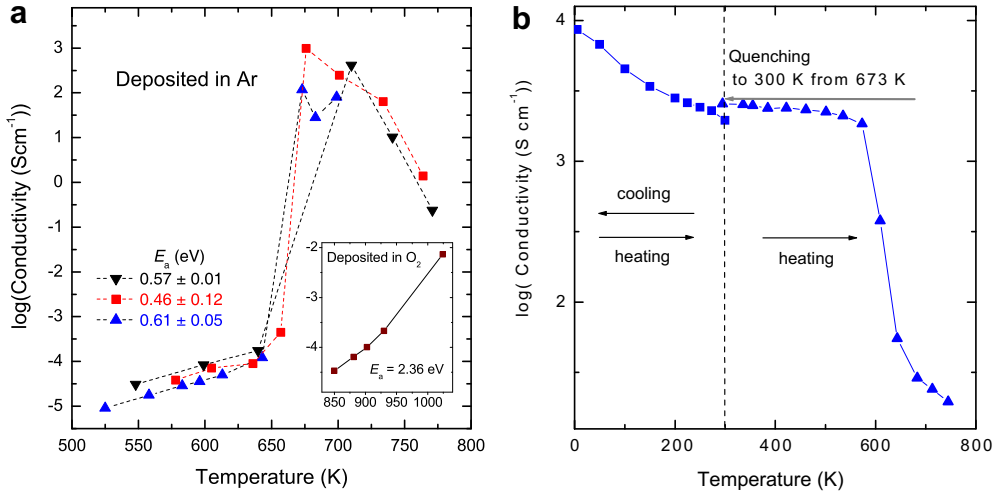

Fig. 21. (a) Conductivity as a function of temperature of gallium oxide films that were prepared in argon atmosphere (symbols). The inset shows the conductivity of a film prepared in pure O_2. (b) Conductivity of a gallium oxide film, that was prepared in Ar, heated quickly to $T = 673$ K, which is just above the insulator–metal transition temperature, and quenched subsequently to $T = 300$ K. Adapted by permission from Macmillan Publishers Ltd: Nature Materials, Ref. [64], copyright (2008).

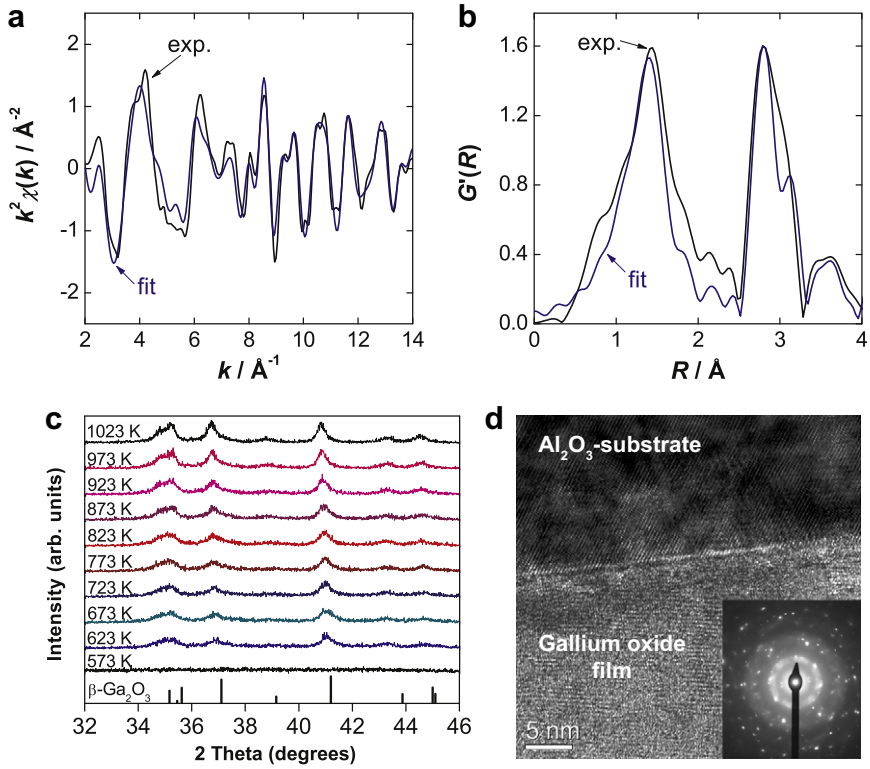

Fig. 22. (a) EXAFS, $k^2 \cdot \chi(k)$, of an as-prepared, amorphous gallium oxide film at the Ga *K*-edge. (b) Modified radial distribution function $G'(R)$ (Fourier transform of the EXAFS in panel (a) (black lines = experimental data, blue lines = fit, see text). (c) *in situ* X-ray diffraction patterns taken during heating of the film from RT to 1023 K. (d) Cross-sectional high-resolution transmission electron microscopy (HRTEM) picture of a film that was annealed at 673 K and then quenched to 300 K, showing a sharp interface between the alumina substrate and the gallium oxide film. The inset displays a selected area electron diffraction pattern (SAED) of the gallium oxide film. Reprinted by permission from Macmillan Publishers Ltd: Nature Materials, Ref. [64], copyright (2008).

0.47:0.50:0.03 (nitrogen), i.e. significant gallium excess. Films prepared in oxygen are transparent, films prepared in nitrogen are less transparent, while films prepared in Ar are black.

The surface roughness of the films was examined with an interference microscope. The films were found to be uniformly flat with a roughness of ~5 nm.

A typical SIMS depth profile of a two-layered Ga_2O_3 film deposited first in a N_2 and subsequently in an O_2 atmosphere [$Ga_2O_3(O_2)/Ga_2O_3(N_2)/Al_2O_3$] is shown in Fig. 20a. The nitrogen containing secondary ions such as NH^-, $^{14}N^{16}O^-$, $^{14}N^{16}O_2^-$, and $^{69}Ga^{14}N^-$ are seen only in the gallium oxide layer deposited in the N_2 atmosphere thereby confirming the incorporation of nitrogen into the gallium oxide. The depth profiles of NH^-, $^{14}N^{16}O^-$, $^{14}N^{16}O_2^-$ and $^{69}Ga^{14}N^-$ show that nitrogen is homogeneously distributed throughout the depth of the layer. Fig. 20b shows that the intensities of $^{71}Ga_2^{16}O_2^-$ and $^{71}Ga^{16}O_2^-$ signals in the nitrogen doped gallium oxide layer are slightly lower than in the pure gallium oxide layer. This may be possibly due to (i) a matrix effect which may cause a change in the secondary ion yield or (ii) the replacement of O by N in the nitrogen doped layer. By considering the latter assumption, it is found that ~3% of oxygen has been replaced by nitrogen. This is in good agreement with the results of the EPMA analysis carried out for the GaO_xN_y sample which shows a nitrogen concentration of ~3 at.%.

5.3. Electrical conductivity and insulator–metal transition

All as-prepared films are electrical insulators at room temperature. During heating in an inert atmosphere we observe, however, a marked insulator–metal transition for the films prepared in Ar and N_2. As an example, Fig. 21a shows results for films prepared in Ar. The films exhibit semiconducting behaviour with a small activation energy of about 0.55 eV below the insulator–metal transition temperature, $T_{IM} \approx 663$ K. The conductivity increases sharply by 7 orders of magnitude at about 663 K, and at 673 K the conductivity is already as high as 10^3 S cm^{-1}. During further heating the conductivity decreases again. No conductivity jump was found for the amorphous, but stoichiometric gallium oxide which was prepared in oxygen. Its conductivity is much smaller (inset in Fig. 21a) and increases continuously with increasing temperature with a much higher activation energy of 2.36 eV.

By quenching the sample to 300 K immediately after the transition, the highly conducting state can be frozen in. During cooling down to temperatures of 5 K (Fig. 21b) the conductivity increases, confirming that the sample in the highly conducting state indeed exhibits metallic behaviour with a conductivity at $T = 5$ K of $8.6 \cdot 10^3$ S cm^{-1}. Upon subsequent heating in an inert argon atmosphere the high conductivity is retained up to a temperature of 600 K, above which it decreases sharply.

5.4. Structural characterization

The as-deposited gallium oxide films are X-ray amorphous (see Fig. 22c). To investigate their local structure we employed XAS at the Ga *K*-edge (Fig. 22a and b). Modeling of the EXAFS with FEFF8 [69] indicates that the *local* structure around gallium atoms can be described reasonably well by the same oxygen coordination polyhedra as in crystalline β-Ga_2O_3, i.e. strongly distorted oxygen octahedra and tetrahedra. But in contrast to β-Ga_2O_3 that has equal amounts of gallium atoms with octahedral and tetrahedral oxygen coordination (see Table 1), the amorphous, highly non-stoichiometric gallium oxide $Ga_{0.45}O_{0.55}$ contains a significantly higher

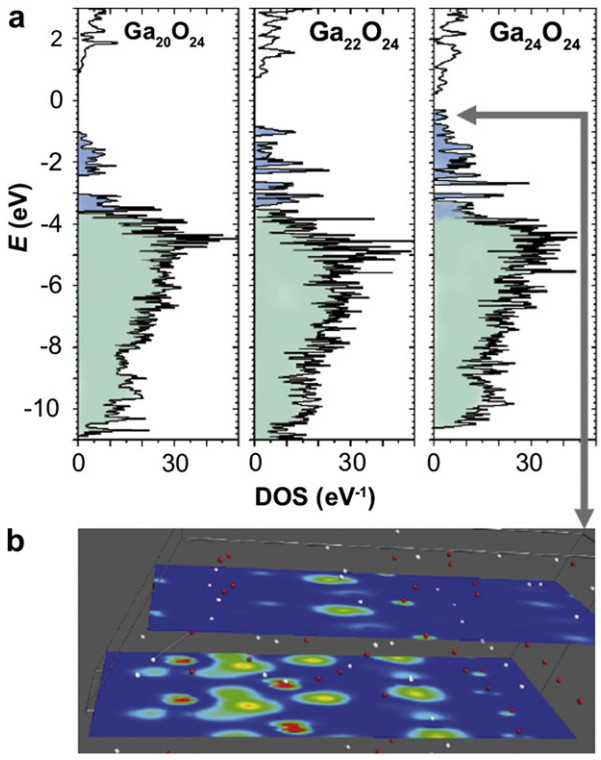

Fig. 23. Electronic structure of supercells $Ga_{20}O_{24}$, $Ga_{22}O_{24}$, and $Ga_{24}O_{24}$. (a) Density of states (DOS) calculated with the B3LYP functional. The states from the O 2p like valence states to the bottom of the conduction bands are displayed. The occupied states are colored (light = valence states, dark = defect states). (b) Electron density distribution of the uppermost occupied defect states of Ga_I in $Ga_{24}O_{24}$ (states at $E \approx -0.5$ eV in panel a) for two lattice planes. Ga_I is located in the lower plane and at these concentrations of Ga_I the character of the defect states changes from localized to non-localized. Reprinted by permission from Macmillan Publishers Ltd: Nature Materials, Ref. [64], copyright (2008).

fraction of gallium atoms with tetrahedral oxygen coordination, Ga_{tet}:Ga_{oct} ≈ 0.57:0.43 (Fig. 22a and b). As the EXAFS analysis shows that the amorphous samples exhibit a well defined short range order, the concept of point defects, which is strictly speaking only valid for crystalline structures, is applicable to our amorphous gallium oxide as well. In this sense, the gallium excess of $Ga_{0.45}O_{0.55}$ compared to β-Ga_2O_3 can be due to gallium interstitials, Ga_I, and/or oxygen vacancies, V_O. Both defects are electron donors, and thus, $Ga_{0.45}O_{0.55}$ can be regarded formally as a heavily donor-doped semiconductor.

To investigate possible structural changes near the insulator–metal transition we utilized *in situ* X-ray diffraction during heating an as-prepared film in an inert atmosphere from room temperature (RT) to 1023 K. The films are X-ray amorphous from RT up to 573 K (Fig. 22c). At 623 K broad peaks appear that can be assigned to β-Ga_2O_3. This means that crystallization of β-Ga_2O_3 starts within the amorphous gallium oxide at least 40 K *below* the insulator–metal transition temperature. Fig. 22d shows a high-resolution transmission electron micrograph (HRTEM) and a selected area electron diffraction (SAED) pattern of a sample that was quenched from $T = 673$ K to $T = 300$ K. The d-spacings calculated from the diffraction peaks and the diffuse background confirm that the film consists of a mixture of crystalline β-Ga_2O_3 and an amorphous gallium oxide.

5.5. Chemically induced insulator–metal transition

Amorphous gallium oxide with gallium excess, GaO_x, can be regarded as a heavily donor-doped semiconductor. If the donors form new electronic states above the valence states we expect a decreasing band gap. Since the films prepared in Ar are black in the as-prepared state, the optical band gap is already small enough for strong optical absorption in the visible and near infrared range (VIS, NIR) to occur. On the other hand, the as-prepared samples are still insulators, despite their large gallium excess. Thus, the donor concentration in the as-prepared samples is still below the critical donor concentration for closing the band gap (which we correlate with the insulator–metal transition at 673 K). To understand why the donor concentration in the amorphous oxide GaO_x increases during heating we recall that about 40 K below the insulator–metal transition temperature crystallization of stoichiometric β-Ga_2O_3 starts (Fig. 22). This reaction can be described by:

$$GaO_x(\text{amorphous}) \rightarrow Ga_{1-2b}O_{x-3b}(\text{amorphous}) + b \cdot ß - Ga_2O_3(\text{crystalline}) \quad \text{(II)}$$

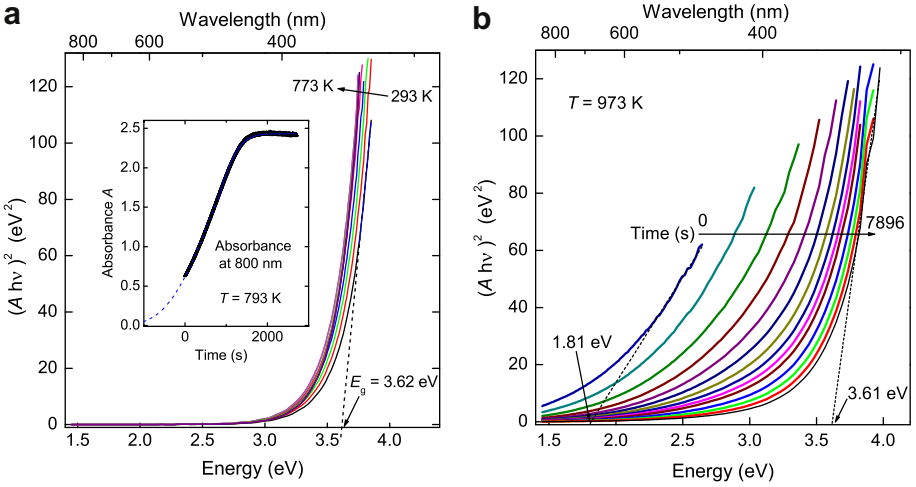

Fig. 24. *In situ* optical absorption of a gallium oxide film deposited in nitrogen. The quantity $(A\ h\nu)^2$ is plotted against the photon energy $h\nu$ (A = absorption). a) Optical absorption spectra during heating from RT to 773 K. The optical band gap at RT is $E_g = 3.62$ eV. The inset shows the absorbance, A, at a fixed wavelength of 800 nm as function of time after heating an as-prepared sample rapidly to 793 K (black symbols = experimental data, dashed line = fit with Eq. (3)). (b) Optical absorption spectra taken as a function of time after blackening at 793 K (inset in panel a) and subsequent fast heating to 973 K. Adapted by permission from Macmillan Publishers Ltd: Nature Materials, Ref. [64], copyright (2008).

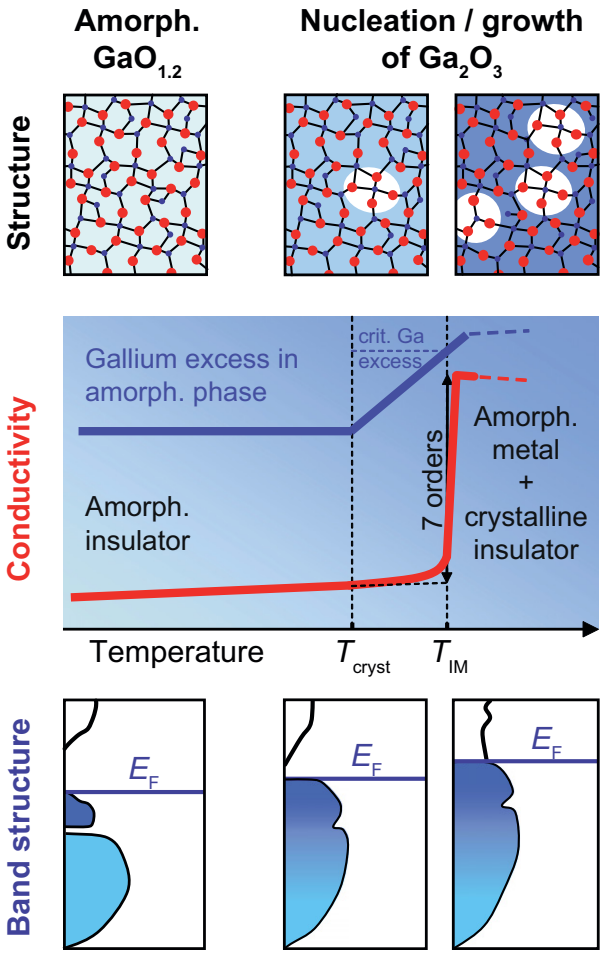

Fig. 25. Schematic illustration of the correlation between geometrical structure, gallium excess, electrical conductivity, and band structure of highly non-stoichiometric, amorphous gallium oxide as a function of temperature. Reprinted by permission from Macmillan Publishers Ltd: Nature Materials, Ref. [64], copyright (2008).

Here b is the amount of stoichiometric β-Ga_2O_3 that is formed during crystallization. During reaction (II) the gallium excess in the remaining amorphous matrix increases further because the formation of β-Ga_2O_3 requires more oxygen than gallium, Eventually, the donor concentration in amorphous GaO_x is driven above the critical value for which the band gap is closed and the amorphous oxide becomes metallic. Reaction (II) thus describes an internal redox reaction or a disproportionation that takes place *within* the metastable, amorphous gallium oxide matrix with gallium excess. The high thermodynamic stability of crystalline, stoichiometric β-Ga_2O_3 is the driving force for this internal reaction. No external gas phase oxygen participates in this reaction, as all annealing experiments were conducted in oxygen-free atmospheres. The behaviour of N-doped gallium oxides, GaO_xN_y will be discussed in Section 5.6.

To confirm that the band gap of gallium oxide decreases with increasing gallium excess we have calculated the electronic structure of (lattice relaxed) highly non-stoichiometric gallium oxide by means of DFT using two functionals, GGA [70] and B3LYP [71]. These calculations show that gallium interstitials, Ga_I, and oxygen vacancies, V_O, both produce defect states in the band gap of Ga_2O_3. For the gallium interstitial we find inside the band gap two new localized states/bands that are occupied by the three valence electrons of the extra Ga atom [64]. For an oxygen vacancy we find a color centre occupied by two electrons. The charge density is highly localized at the oxygen vacancy and the neighboring Ga ions; more importantly, the states are much closer to the valence band. Consequently, these results strongly suggest that, since we require the band gap to close for the insulator–metal transition, the amorphous phase may be considered more appropriately as containing gallium interstitials (donor states close to the conduction band) rather than oxygen vacancies (donor states close to the valence band). We emphasize, though, that the disproportionation reaction (II) does not depend on the nature of the dominating defect.

By increasing the Ga-excess the number of states in the original optical band gap increases and the energy gap between the highest occupied states and the lowest conduction states decreases. In Fig. 23a we have plotted the DOS for the supercells $Ga_{20}O_{24}$, $Ga_{22}O_{24}$, and $Ga_{24}O_{24}$. The composition $Ga_{20}O_{24}$ corresponds to the composition of the as-prepared film, $Ga_{0.45}O_{0.55}$. The energy gap between the valence states and the unoccupied states in the conduction band is ≈4.5 eV (see DOS of $Ga_{20}O_{24}$), in fair agreement with the experimental value of 4.9 eV for β-Ga_2O_3 (as expected for the functional B3LYP). With increasing gallium excess the valence electron states and the defect states start to overlap energetically, the optical band gap decreases from 1.9 eV for $Ga_{20}O_{24}$ to 0.5 eV for $Ga_{24}O_{24}$, and the highest occupied states change their character from localized to non-localized electron states. Due to i) the high number of defects, ii) the resulting lattice relaxation, and iii) the experimental EXAFS results we believe that our calculated electronic structure describes the essential electronic features of the amorphous oxide in an appropriate way (except for band tailing and the related mobility edges [72,73]). Nevertheless, we cannot predict for two reasons the exact Ga concentration at which the transition from isolating to semi-metallic and metallic behaviour should occur. First, the structure optimization for these systems has been performed assuming triclinic translation symmetry, and second, even for hybrid functionals, such as B3LYP, the calculated band gaps differ from experiment.

5.6. *In situ optical absorption of nitrogen doped gallium oxide*

Films deposited in a pure nitrogen atmosphere contain several at.% of nitrogen and exhibit gallium excess too. They have a typical composition Ga:O:N of 0.47:0.50:0.03 and are also X-ray amorphous. As the films prepared in argon, they show an insulator–metal transition, but now the conductivity jump is smaller (roughly 5 orders of magnitude) and occurs at higher temperatures ($T \approx 773$ K). Crystallization of β-Ga_2O_3 in the N-doped films starts also at higher temperatures (between 723 K and 773 K) than in films prepared in Ar.

But in contrast to films prepared in Ar which are black, as-prepared N-doped films are still transparent. This is probably due the fact that nitrogen is expected to substitute for oxygen, thus acting as an acceptor and compensating some of the donor defects, and hence it lowers the Fermi energy resulting in a larger optical band gap. This allows us to further investigate the Ga–O (N) system near the metal-insulator transition by means of *in situ* optical absorption spectroscopy. Fig. 24a depicts absorption spectra, from which the optical band gap E_g was determined as the intercept of the tangent at high energies with the energy axis [74]. For an as-prepared, N-doped film the optical band gap, $E_g = 3.62$ eV, is smaller than the gap of 4.9 eV in crystalline β-Ga_2O_3 due to the additional states in the band gap (gallium excess) and, in addition, due to band tailing that is caused by the strong chemical and structural disorder [74]. Upon heating up to $T = 773$ K the absorption spectrum changes only slightly. However, during further heating, shortly above 773 K, the absorption increases rapidly and the film turns completely black. The blackening kinetics (inset in Fig. 24a) can be described well by JMAK kinetics [44] (see Equation (3)). The exponent n is initially 4 (constant nucleation rate

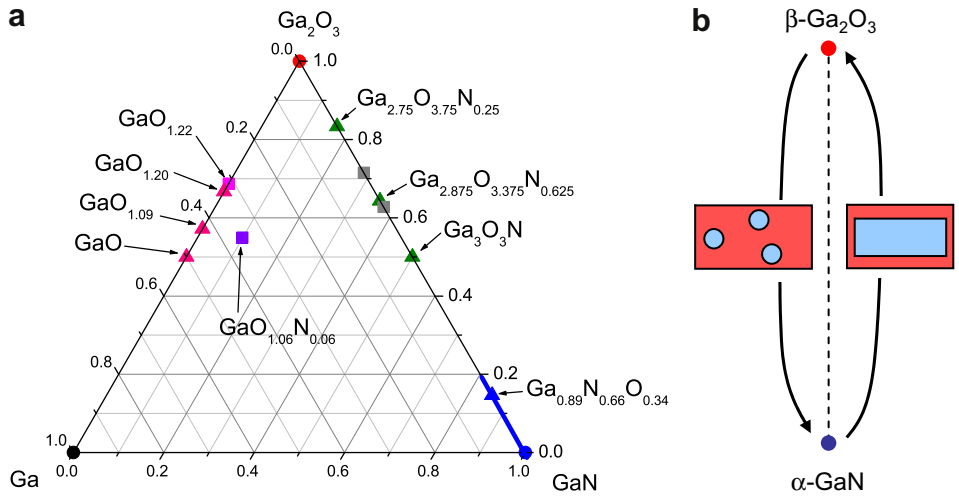

Fig. 26. (a) Gibbs triangle Ga–GaN–Ga_2O_3. Squares indicate new, experimentally observed compounds, gallium deficient spinels $Ga_{3-z}(O,N)_4$ [52,53] and gallium excess amorphous compounds GaO_xN_y [64]. Triangles indicate compounds that were investigated by density-functional theory calculations, γ-galons [50], nitrogen-rich gallium oxynitrides [59], and gallium excess amorphous compounds GaO_x [64]. (b) Schematic illustration of the ammonolysis of Ga_2O_3 with nucleation and growth of GaN nuclei and the oxidation of GaN with layered growth of Ga_2O_3 [33]. (For interpretation of the references to color in this figure legend, the reader is referred to the web version of this article.)

of β-Ga_2O_3) and changes after about 800 s to 3 (rate determining step at the interface between the matrix and the growing precipitate), while the rate constant k changes only slightly from $k = 3.5 \cdot 10^{-4}\ s^{-1}$ to $k = 7 \cdot 10^{-4}\ s^{-1}$. We note that the temperature at which the film becomes black is essentially identical to the insulator–metal transition temperature and slightly higher than the temperature where crystallization of β-Ga_2O_3 starts. As the "blackening" cannot be due to β-Ga_2O_3, which is transparent (band gap 4.9 eV), the remaining amorphous gallium oxide must have become a strong optical absorber.

On heating the blackened film further to 973 K the film becomes again transparent. This de-blackening at elevated temperatures is due to oxidation of the excess gallium in the amorphous part of the film by residual oxygen from the surrounding atmosphere. Once the gallium excess in the amorphous matrix has decreased below the critical value, the band gap opens up again resulting in the de-blackening. The first optical spectrum that we were able to measure *in situ* after heating the blackened film to 973 K yields already a small optical band gap, $E_g \approx 1.8$ eV (Fig. 24b). During further de-blackening the optical band gap increases continuously to about 3.6 eV (Fig. 24b) and eventually the film is again transparent. After long term annealing the band gap approaches the value 4.9 eV for β-Ga_2O_3. The underlying oxidation by residual oxygen from the surrounding atmosphere explains also the strong decrease of the conductivity at elevated temperatures (Fig. 21).

The optical absorption experiments confirm that the band gap in the as-prepared N-doped gallium oxide is still too large for optical absorption in the VIS–NIR range, despite the large gallium excess. Crystallization of β-Ga_2O_3 increases the gallium excess in the remaining amorphous matrix and leads to a decreasing band gap that is eventually small enough for complete optical absorption in the VIS–NIR range. Finally, the band gap is closed and the sample exhibits an insulator–metal transition. These results also indicate that by means of doping tuning of the insulator–metal transition temperature is possible.

5.7. Correlation of structure, gallium excess, electronic structure and conductivity

The scheme in Fig. 25 summarizes our experimental and theoretical findings for non-stoichiometric and amorphous gallium oxide. It demonstrates that the insulator–metal transition is correlated with a transition from an amorphous oxide of uniform composition to a heterogeneous system that consists of an amorphous oxide and a crystalline oxide of the same element, but of different chemical composition.

At low temperatures (left column in Fig. 25) the non-stoichiometric oxide $GaO_{1.2}$ is amorphous with a short range order where Ga (blue) is tetrahedrally and octahedrally coordinated by oxygen (red) (as determined by EXAFS). The shown geometrical structure is a schematic, two-dimensional cut through the amorphous structure. The conductivity is low with a small activation energy corresponding to the gap (lower row) between the defect states (gallium excess) and the conductivity band (or the mobility edge). At the temperature T_{cryst} nucleation and growth of crystalline, stoichiometric β-Ga_2O_3 (white nucleus) starts (as determined by *in situ* XRD and *in situ* optical spectroscopy), resulting in an increasing gallium excess in the remaining amorphous oxide. Due to the increasing Fermi energy, E_F, and the decreasing band gap the conductivity increase is now steeper than below T_{cryst}. Eventually, at the temperature T_{IM} a critical number of β-Ga_2O_3 nuclei and a critical gallium excess in the remaining amorphous gallium oxide is reached; the band gap is closed and the conductivity jumps by seven orders of magnitude (insulator–metal transition). Possible applications of this insulator–metal transition for non-volatile storage devices are discussed in Ref. [64].

6. Conclusions

In this paper we have summarized our recent experimental and theoretical results on the thermodynamics, structure and kinetics in the system Ga–O–N, and we have discussed them in conjunction with results reported in literature.

We examined the ammonolysis of β-Ga_2O_3 in the temperature range of 873–1053 K with *ex situ* X-ray and neutron diffraction and *in situ* X-ray absorption spectroscopy. XRD and neutron diffraction on samples quenched after ammonolysis show that β-Ga_2O_3 and α-GaN are the only crystalline phases that can be detected. Within the detection limit of these methods we find the solubility of nitrogen in crystalline β-Ga_2O_3 to be smaller than 2–3 at.%. From time-resolved, *in situ* X-ray absorption spectra that were taken during

the ammonolysis of Ga_2O_3 we could show that the changes in the electronic structure and the short range order around Ga atoms during the ammonolysis of Ga_2O_2 proceed with the same speed. The kinetics of the ammonolysis of Ga_2O_3 can be described well by a Johnson–Mehl–Avrami–Kolmogorow model with an Avrami exponent of ~3 indicating a reaction mechanism with closed nucleation and 3-dimensional growth of GaN nuclei. The rate determining step of the reaction is the formation of the newly formed GaN phase at the interface between the GaN nuclei and the Ga_2O_3 matrix. The oxidation kinetics of GaN can be modeled by a shrinking core model where the rate determining step is again the interfacial formation of the newly formed gallium oxide product phase.

We investigated the structure and enthalpy of formation of spinel-type gallium oxynitrides, γ-galons, within density-functional theory. The results show that the ternary oxynitride will exhibit a defective structure, with octahedral vacancies within the cation sublattice. Both the lattice parameter and the band gap of cubic γ-galons depend almost linearly on the GaN content. The enthalpy of formation of the ternary spinel from the binary compounds β-Ga_2O_3 and wurtzite GaN is, however, positive. Thus, substantial contributions arising from the entropy of mixing within the anion sublattice and, in addition, elevated pressures are needed to stabilize γ-galons.

By means of PLD we were able to prepare highly non-stoichiometric, amorphous gallium oxide with a strong Ga-excess (e.g. $GaO_{1.2}$). At a temperature around 670 K we found an insulator–metal transition, with a conductivity jump of seven orders of magnitude. Through experimental studies and density-functional theory calculations we could demonstrate that the conductivity jump takes place at a critical gallium concentration and is induced by crystallization of stoichiometric β-Ga_2O_3 within the metastable oxide matrix. By doping with nitrogen the critical temperature and the conductivity in the highly conducting state can be tuned.

In Fig. 26 we aim to summarize our findings concerning the thermodynamics and kinetics. The phase diagram in Fig. 26a shows again the ternary system Ga–O–N that was already shown in Fig. 1. But now we focus on the Ga-rich part of the diagram which is defined by the corners Ga, GaN, and Ga_2O_3. In comparison to Fig. 1, the phase diagram contains new compounds, the spinel-type γ-galons, and the amorphous gallium oxides with gallium excess. As the latter ones exhibit a pronounced insulator–metal transition upon heating, the question arises whether it is possible to increase the Ga-excess and to extend the area of non-stoichiometric gallium oxides and/or oxynitrides. Finally, Fig. 26b depicts schematically our results on the kinetics of the ammonolysis of Ga_2O_3 and the oxidation of GaN. While the former one is characterized by nucleation and growth of GaN, the latter one is characterized by a layered growth of Ga_2O_3.

Acknowledgement

Financial support by the German Research Foundation (DFG Priority Program 1136, Substitutional Effects in Ionic Solids) is gratefully acknowledged. The authors would like to express their gratitude to A. Shenyshin and M. Hoelzel (FRMII, Garching) for their support during the neutron measurements at the SPODI diffractometer, M. Lerch (FU Berlin) for the quantitative analysis of nitrogen and oxygen via the hot gas extraction method, G. Heger, G. Roth and K. Sparta (AIXTAL, Aachen) for support in all crystallographic matters, E. Welter, K. Rickers, A. Webb and D. Zajac (all HASYLAB @ DESY) for support during the beam times, R. Zaunbrecher for making the SEM measurements, F. Dorn and T. Weirich for recording the TEM micrographs, and B. Huppertz for technical support.

References

[1] Akasaki I, Amano H. Crystal growth and conductivity control of group III nitride semiconductors and their application to short wavelength light emitters. Jpn J Appl Phys 1997;36:5393–408.
[2] Nakamura S, Pearton S, Fasol G. The blue laser diode. The complete story. 2nd ed. Berlin: Springer; 2000.
[3] Fleischer M, Meixner H. Electron mobility in single- and polycrystalline β-Ga_2O_3. J Appl Phys 1993;74:300–5.
[4] Lorenz MR, Woods JF, Gambino RJ. Some electrical properties of the semiconductor β-Ga_2O_3. J Phys Chem Solids 1976;28:403–4.
[5] Harwig T, Wubs GJ, Dirksen GJ. Electrical properties of β-Ga_2O_3 single crystals. Solid State Commun 1976;18:1223–5.
[6] Kinski I, Scheiba F, Riedel R. Advances in gallium oxonitride ceramics: a new class of materials in the system Ga–O–N. Adv Eng Mater 2005;7:921–7.
[7] Slack GA, Schowalter LJ, Morelli D, Freitas Jr JA. Some effects of oxygen impurities on AlN and GaN. J Cryst Growth 2002;246:287–98.
[8] Chen WM, Buyanova IA, Wagner M, Monemar B, Lindström LJ, Amano H, et al. Role of the substitutional oxygen donor in the residual n-type conductivity in GaN. MRS Internet J Nitride Semicond Res 1999;4S1(G5.4).
[9] Wetzel C, Amano H, Akasaki I, Ager JW, Grzegory I, Meyer BK. DX-like behavior of oxygen in GaN. Physica B 2001;302–303:23–38.
[10] Korotkov RY, Wessels BW. Electrical properties of oxygen doped GaN grown by metalorganic vapor phase epitaxy. MRS Internet J Nitride Semicond Res 2000;5S1(W3.80).
[11] Chung BC, Gershenzon M. The influence of oxygen on the electrical and optical properties of GaN crystals grown by metalorganic vapor phase epitaxy,. J Appl Phys 1992;72:651–9.
[12] Van de Walle CG. Effects of impurities on the lattice parameters of GaN. Phys Rev B 2003;68:165209.
[13] Pankove JI, Wang HL, Bachmann KJ, Schwab C, editors. Non-stoichiometry in semiconductors. Elsevier Science; 1992.
[14] Roy R, Hill VG, Osborn EF. Polymorphism of Ga_2O_3 and the system Ga_2O_3–H_2O. J Am Chem Soc 1952;74:719–22.
[15] Zinkevich M, Aldinger F. Thermodynamic assessment of the gallium-oxygen system. J Am Ceram Soc 2004;87:683–91.
[16] Åhman J, Svensson G, Albertsson J. A reinvestigation of β-gallium oxide. Acta Crystallogr C 1996;52:1336–8.
[17] Barin I. Thermochemical data of pure substances. Weinheim: VCH Publishers Inc.; 1995.
[18] Tippins HH. Optical absorption and photoconductivity in the band edge of β-Ga_2O_3. Phys Rev 1965;140:A316–9.
[19] Binet L, Gourier D. Origin of the blue luminescence of β-Ga_2O_3. J Phys Chem Solids 1998;59:1241–9.
[20] Ogita M, Higo K, Nakanishi Y, Hatanaka Y. Ga_2O_3 thin film for oxygen sensor at high temperature. Appl Surf Sci 2001;175–176:721–5.
[21] Orita M, Ohta H, Hirano M, Hosono H. Deep-ultraviolet transparent conductive β-Ga_2O_3 thin films. Appl Phys Lett 2000;77:4166–8.
[22] Cho S, Lee J, Park I, Kim S. New luminescence band due to nitrogen impurities in gallium oxide powders. Mater Lett 2002;57:1004–9.
[23] Fleischer M, Hoellbauer L, Born E, Meixner H. J Am Ceram Soc 1997;80:2121–5.
[24] Bartic M, Baban CI, Suzuki H, Ogita M, Isai M. β-Gallium oxide as oxygen gas sensors at a high temperature. J Am Ceram Soc 2007;90:2879–84.
[25] Ambacher O. Growth and applications of group III-nitrides. J Phys D: Appl Phys 1998;31:2653–711.
[26] Juza R, Hahn H. Über die Kristallstrukturen von Cu_3N, GaN und InN. Z Anorg Allg Chem 1938;239:282–7.
[27] Balkas CM, Davis RF. Synthesis routes and characterization of high-purity, single-phase gallium nitride powders. J Am Ceram Soc 1996;79:2309–12.
[28] Pearton SJ, Ren F. GaN electronics. Adv Mater 2000;12:1571–80.
[29] Schwenzer B, Hu J, Seshadri R, Keller S, den Baars SP, Mishra UK. Gallium nitride powders from ammonolysis: influence of reaction parameters on structure and properties. Chem Mater 2004;16:5088–95.
[30] Park YJ, Oh CS, Yeom TH, Yu YM. Ammonolysis of β-Ga_2O_3 and its application to the sublimation source for the growth of GaN film. J Cryst Growth 2004;264:1–6.
[31] Jung WS. Reaction intermediate(s) in the conversion of β- gallium oxide to gallium nitride under a flow of ammonia. Mater Lett 2002;57:110–4.
[32] Roehrens D, Brendt J, Samuelis D, Martin M. On the ammonolysis of Ga_2O_3: an XRD, neutron diffraction and XAS investigation of the oxygen rich part of the system Ga_2O_3–GaN. J Solid State Chem, submitted for publication
[33] Brendt J, Samuelis D, Weirich TE, Martin M. An in situ XAS investigation of the kinetics of the ammonolysis of Ga_2O_3 and the oxidation of GaN. Phys Chem Chem Phys 2009;11:3127–37.
[34] Rodriguez-Carvajal J. Recent advances in magnetic structure determination by neutron powder diffraction. Physica B 1993;192:55–69.
[35] Koops U, Hesse D, Martin M. High-temperature oxidation of CoGa: influence of the crystallographic orientation on the oxidation rate. J Mater Res 2002;17:2489–98.

[36] Hilbrandt N, Martin M. A quantitative in situ Fe-K XAFS study (T > 1270 K) on the oxidation degree of iron in ($Mg_{1-x}Fe_x$)O. J Synchrotron Radiat 1999;6:489–91.
[37] Frahm R. New method for time dependent X-ray absorption studies. Rev Sci Instrum 1989;60:2515–8.
[38] Ravel B. Athena user's guide 1.0; 2007.
[39] Koningsberger DC, Prins R. X-ray absorption: principles, applications, techniques of EXAFS, SEXAFS and XANES. New York: Wiley-Interscience; 1988.
[40] Newville M, Livins P, Yacoby Y, Rehr JJ, Stern EA. Near-edge X-ray-absorption fine structure of Pb: a comparison of theory and experiment. Phys Rev B 1993;47:14126–31.
[41] Avrami M. Kinetics of phase change. I. General theory. J Chem Phys 1939;7:1103–12.
[42] Avrami M. Kinetics of phase change. II. Transformation-time relations for random distribution of nuclei. J Chem Phys 1940;8:212–24.
[43] Avrami M. Granulation, phase change, and microstructure, kinetics of phase change. III. J Chem Phys 1941;9:177–84.
[44] Burke J. The kinetics of phase transformations in metals. Pergamon Press; 1965.
[45] Humphreys FJ, Hatherly M. Recrystallisation and related annealing phenomena. Elsevier; 2004.
[46] Deininger C, Egerton RF, Hofer F, Jouffrey B, Krahl D, Leapman RD, et al. In: Reimer L, editor. Energy-filtering transmission electron microscopy. Berlin Heidelberg: Springer; 1995.
[47] Wolter SD, Mohney SE, Venugopalan H, Wickenden AE, Koleske DD. Kinetic study of the oxidation of gallium nitride in dry air. J Electrochem Soc 1998;145:629–32.
[48] McCauley JW, Corbin ND. Phase relations and reaction sintering of transparent cubic aluminium oxynitride spinel (ALON). J Am Ceram Soc 1979;62:476–9.
[49] Puchinger M, Kisailus DJ, Lange FF, Wagner T. Microstructural evolution of precursor-derived gallium nitride thin films. J Cryst Growth 2002;245: 219–27.
[50] Kroll P, Dronskowski R, Martin M. Formation of spinel-type gallium oxynitrides: a density-functional study of binary and ternary phases in the system Ga–O–N. J Mater Chem 2005;15:3296–302.
[51] Kroll P. Spinel-type gallium oxynitrides attainable at high pressure and high temperature. Phys Rev B 2005;72:144407.
[52] Soignard E, Machon D, McMillan PF, Dong J, Xu B, Leinenweber K. Spinel-structured gallium oxynitride (Ga_3O_3N) synthesis and characterization: an experimental and theoretical study. Chem Mater 2005;17:5465–72.
[53] Kinski I, Miehe G, Heymann G, Theissmann R, Riedel R, Huppertz H. High-pressure synthesis of a gallium oxonitride with a spinel-type structure. Z Naturforsch 2005;60b:831–6.
[54] Fang CM, Metselaar R, Hintzen HT, de With G. Structure models for γ-aluminium oxynitride from ab initio calculations. J Am Ceram Soc 2001;84:2633–7.
[55] Adams I, AuCoin TR, Wolff GA. Luminescence in the system Al_2O_3–AlN. J Electrochem Soc 1962;109:1050–4.
[56] McCauley JW. A simple model for aluminium oxynitride spinels. J Am Ceram Soc 1978;61:372–3.
[57] Pisch A, Schmid-Fetzer R. In situ decomposition study of GaN thins films. J Cryst Growth 1998;187:329–32.
[58] Lorenz MR, Binkowski BB. Preparation, stability, and luminescence of gallium nitride. J Electrochem Soc 1962;109:24–6.
[59] Yamamotoa S, Kikkawa S, Masubuchia Y, Takeda T, Wolff H, Dronskowski R, et al. Chemical synthesis, structural elucidation and quantum-chemical modeling of a Cr^{3+} doped gallium oxynitride prepared by precursor nitridation. Solid State Commun 2008;147:41–5.
[60] Kikkawa S, Nagasaka K, Takeda T, Bailey M, Sakurai T, Miyamoto Y. Preparation and lithium doping of gallium oxynitride by ammonia nitridation via a citrate precursor route. J Solid State Chem 2007;180:1984–9.
[61] Kikkawa S, Ohtaki S, Takeda T, Yoshiasa A, Sakurai T, Miyamoto Y. Manganese doped gallium oxynitride prepared by nitridation of citrate precursor. J Alloys Compd 2008;450:152–6.
[62] Shannon RD. Revised effective ionic radii and systematic studies of interatomic distances in halides and chalcogenides. Acta Crystallogr 1976;A32:751–67.
[63] Yamamotoa S, Kikkawa S, Masubuchia Y, Takeda T, Okube M, Yoshiasa A, et al. Preparation of gallium oxynitride in the presence of iron through a citrate route. Mater Res Bull 2009;44:1656–9.
[64] Nagarajan L, De Souza RA, Samuelis D, Valov I, Börger A, Janek J, et al. A chemically driven insulator–metal transition in non-stoichiometric amorphous gallium oxide,. Nat Mater 2008;6:391–8.
[65] Mott NF. Metal–insulator transition. London: Taylor & Francis; 1974.
[66] Gebhard F. The mott metal–insulator transition. Berlin: Springer; 1997.
[67] Chrisey DB, Hubler GK. Pulsed laser deposition of thin films. New York: John Wiley and Sons; 1994.
[68] Wilson RG, Stevie FA, Magee CW. Secondary ion mass spectrometry. New York: John Wiley and Sons; 1989.
[69] Ankudinov AL, Ravel B, Rehr JJ, Conradson SD. Real-space multiple-scattering calculation and interpretation of X-ray-absorption near-edge structure. Phys Rev B 1998;58:7565–76.
[70] Perdew JP, Chevary JA, Vosko SH, Jackson KA, Pederson MR, Singh DJ, et al. Atoms, molecules, solids, and surfaces – applications of the generalized gradient approximation for exchange and correlation. Phys Rev B 1992;46:6671–87.
[71] Becke AD. Density-functional thermochemistry 3. The role of exact exchange. J Chem Phys 1993;98:5648–52.
[72] Anderson PW. Absence of diffusion in certain random lattices. Phys Rev 1958;109:1492–505.
[73] Mott NF. Electrons in disordered structures. Adv Phys 1967;16:49–144.
[74] Tauc J. Amorphous and liquid semiconductors. London: Plenum; 1974.